SUPPLEMENTARY DATA

Fig. S1. Epithelial volume and cell number are unchanged during early pancreatic morphogenesis.

A PdxCre;Nf2$^{f/+}$ X Nf2^{ff}

	Number of *Nf2^{PancKO}*	Number of Het (*Pdx1Cre, Nf2$^{f/+}$*)	Number of controls (*Cre* negative)
Early Pancreatic Organogenesis (E10.5 - E12.5)	97 (25%)	98 (25.3%)	193 (49.7%)
Midgestation (E14.5)	86 (23.2%)	71 (19.2%)	213 (57.6%)
Postnatal P1-P10	48 (18.8%)	58 (22.7%)	126 (58.4%)
4 weeks	19 (18.3%)	26 (25%)	59 (56.7%)

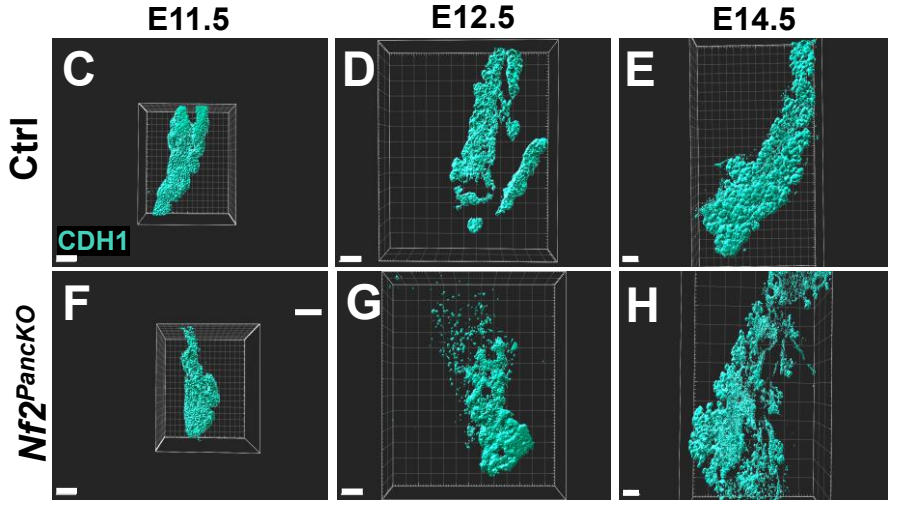

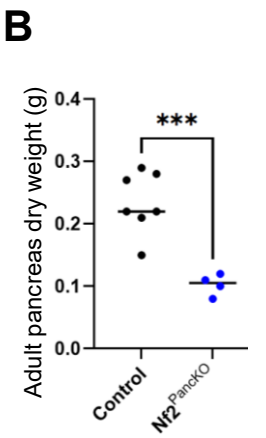

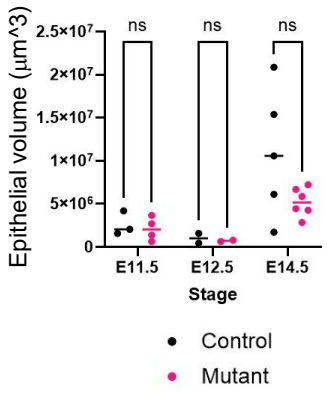

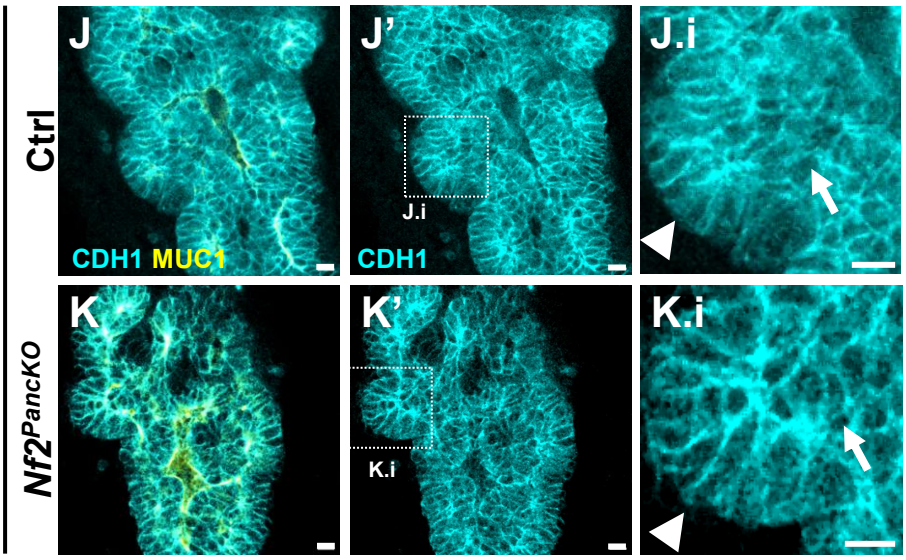

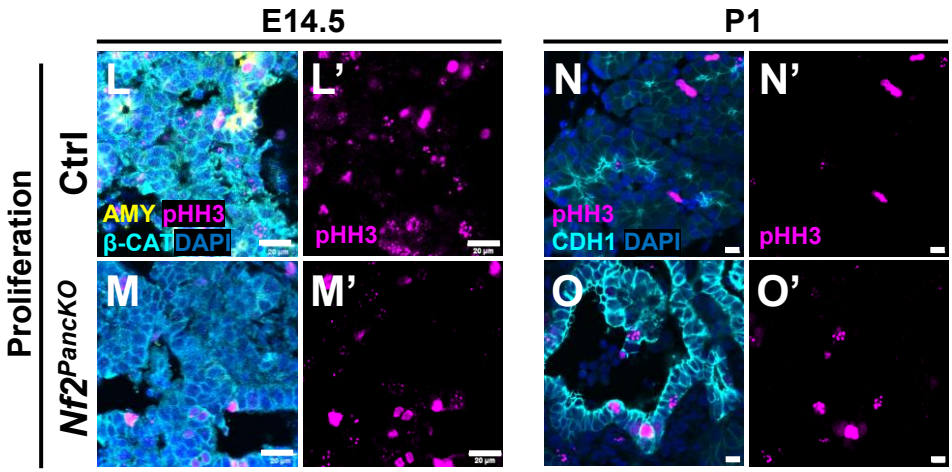

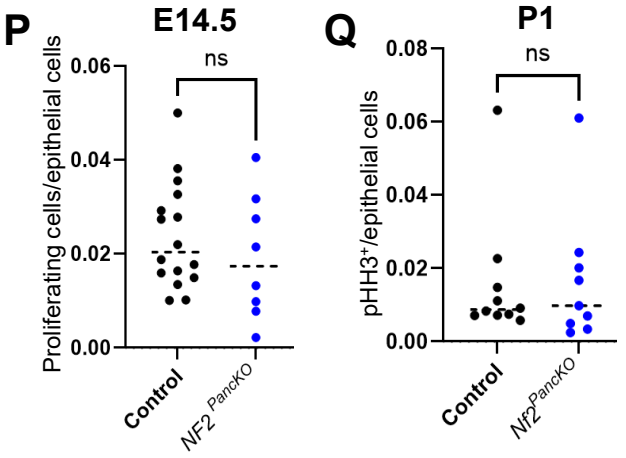

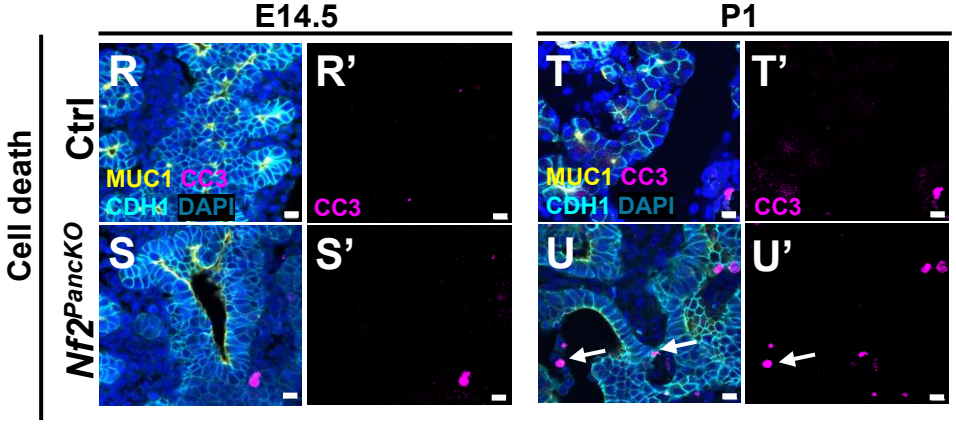

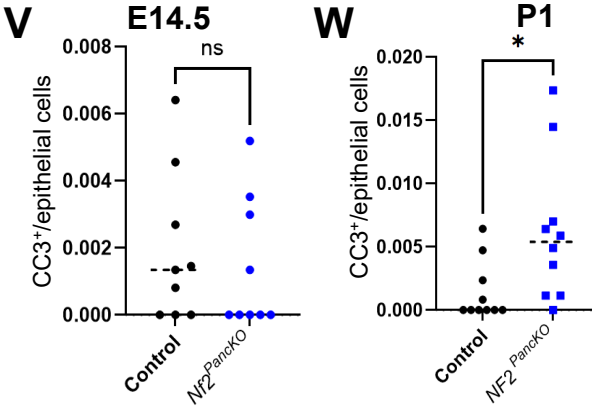

Fig. S1. Epithelial volume and cell number are unchanged during early pancreatic morphogenesis. A) Number of embryos/animals per developmental stage and genotype. Expected Mendelian ratios are 25% *Nf2*^{PancKO}, 25% heterozygous, and 50% Cre-negative control. **B)** Dry weight of adult pancreata. Each dot represents an individual animal, p=0.0002 by Welch's t test. **C-H)** Imaris surface rendering of CDH1^{+} control (C-E), and mutant (F-H) pancreata from E11.5 to E14.5. **I)** Epithelial volume is unchanged during early to mid-pancreatic development in *Nf2*^{PancKO}. Each dot represents one pancreas. **J-K.i')** Representative optical section of E11.5 control and mutant pancreata. White arrowheads, cap cell at periphery of pancreas; white arrows, cuboidal body cell. IF for pHH3, β-catenin and AMY in control **(L, L')** , and **(M, M')** mutant pancreata at E14.5, and **(N-O')** P1**. P)** Quantification of proliferating cells/epithelial cells at E14.5 and **Q)** P1. p=0.40, 0.909, respectively. IF for CC3, CDH1 and MUC1 in control **(R, R')** and mutant **(S, S')** pancreata at E14.5 and **(T-U')** P1**. V)** Quantification of apoptotic cells/CDH1^{+} epithelial cells at E14.5, and **W)** P1. p=0.6448, 0.02, respectively. For panels P,Q,V,W: Each dot represents one FOV analyzed. N=3 ctrl and n=3 *Nf2*^{PancKO} animals analyzed at each embryonic stage. Scale bars: Panels C and F 70μm, D and G 80μm, E and H 700μm, L-O' and R-S' 20μm, and N-O' and T-U' 20μm. For all graphs, line represents median of data.

Fig. S2. Loss of Merlin impairs islet morphology and adult endocrine function.

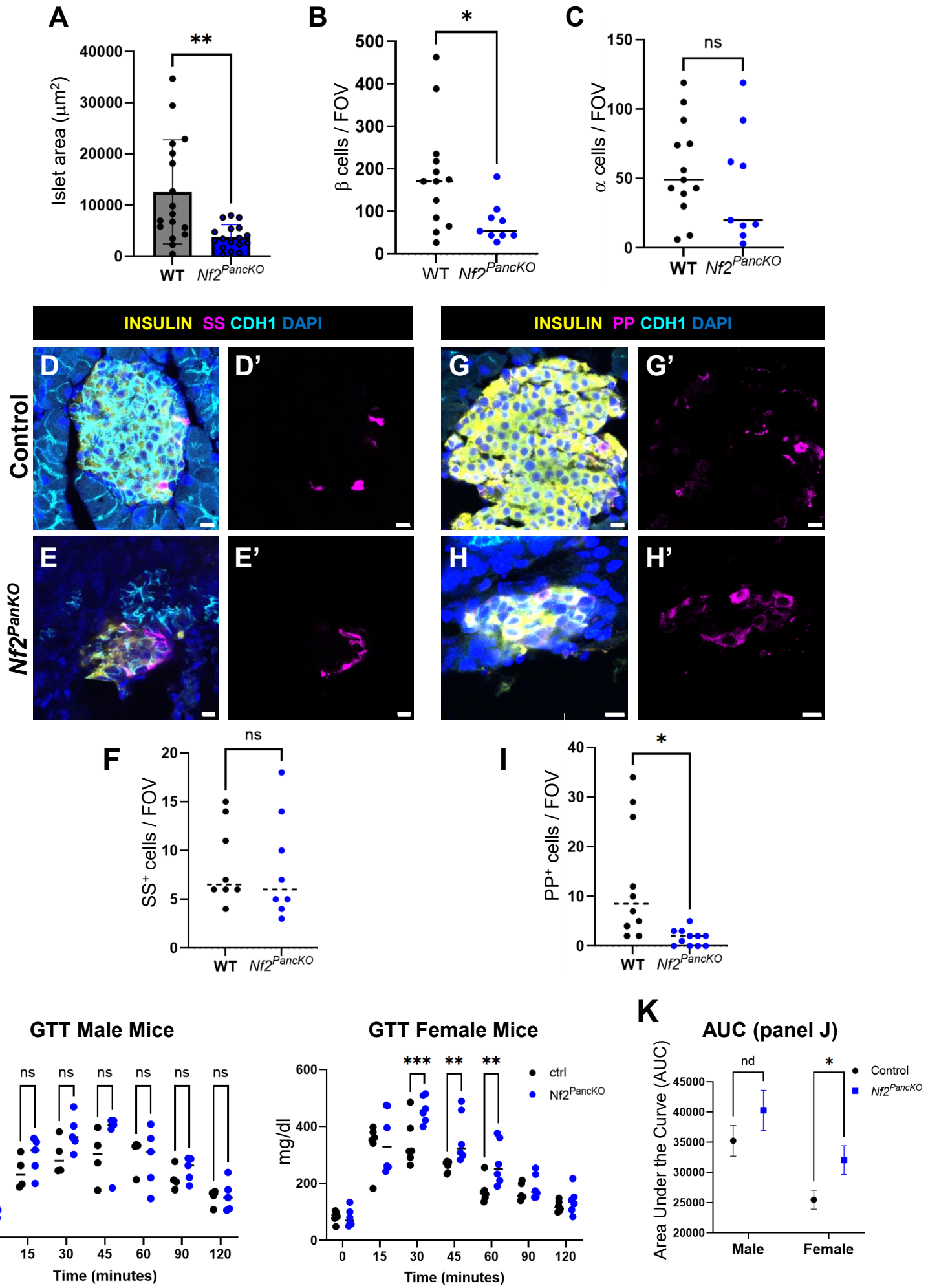

Fig. S2. Loss of Merlin impairs islet morphology and adult endocrine function. **A)** Islet area measured in pancreas sections from control and mutant pancreata as measured on section. P= 0.0015, analyzed by unpaired t-test. Each dot represents one islet. N=17 control, n=17 mutant islets were evaluated from n=3 ctrl and n=3 mutant animals (16-18 weeks). Number of β-cells **(B)** and α-cells **(C)** per field of view (FOV) in adult control and *Nf2*^{PancKO}. P = 0.024, 0.438 respectively, as analyzed by unpaired t-test. For B and C, each dot represents one FOV (13 FOV analyzed from controls, 9 from *Nf2*^{PancKO} , from n=3 ctrl and n=3 mutant pancreata). Representative control **(D, D')** and mutant **(E, E')** tissue stained for insulin, CDH1, and somatostatin (SS). **F)** Somatostatin^{+} cell numbers are not affected by loss of Merlin (p=0.8776). Representative control **(G, G')** and mutant **(H, H')** tissue stained for Insulin, CDH1, and Pancreatic Polypeptide (PP). **I)** PP^{+} cell number is reduced in *Nf2*^{PancKO} adult tissue (p=0.0146). For D-H', each dot represents an FOV, n=3 animals from each genotype, analyzed by Welch's t-test. **J)** Glucose Tolerance (GTT) data in Fig. 1H, separated by sex. Glucose tolerance was unchanged in males, but significantly impaired in females. **K)** Area under the curve (AUC) analysis of glucose tolerance in male and female mice, p = 0.083 for male, 0.00043 for female, analyzed by multiple t tests with Bonferroni-Dunn correction. Scale bars: Panels D-E' and G-H' 10μm. For A-C, F,I,K – line represents median. For K, error bars represent standard deviation.

Fig. S3. Pdx1^{Cre} deletes MERLIN in pancreatic epithelium by E11.5, but not E10.5.

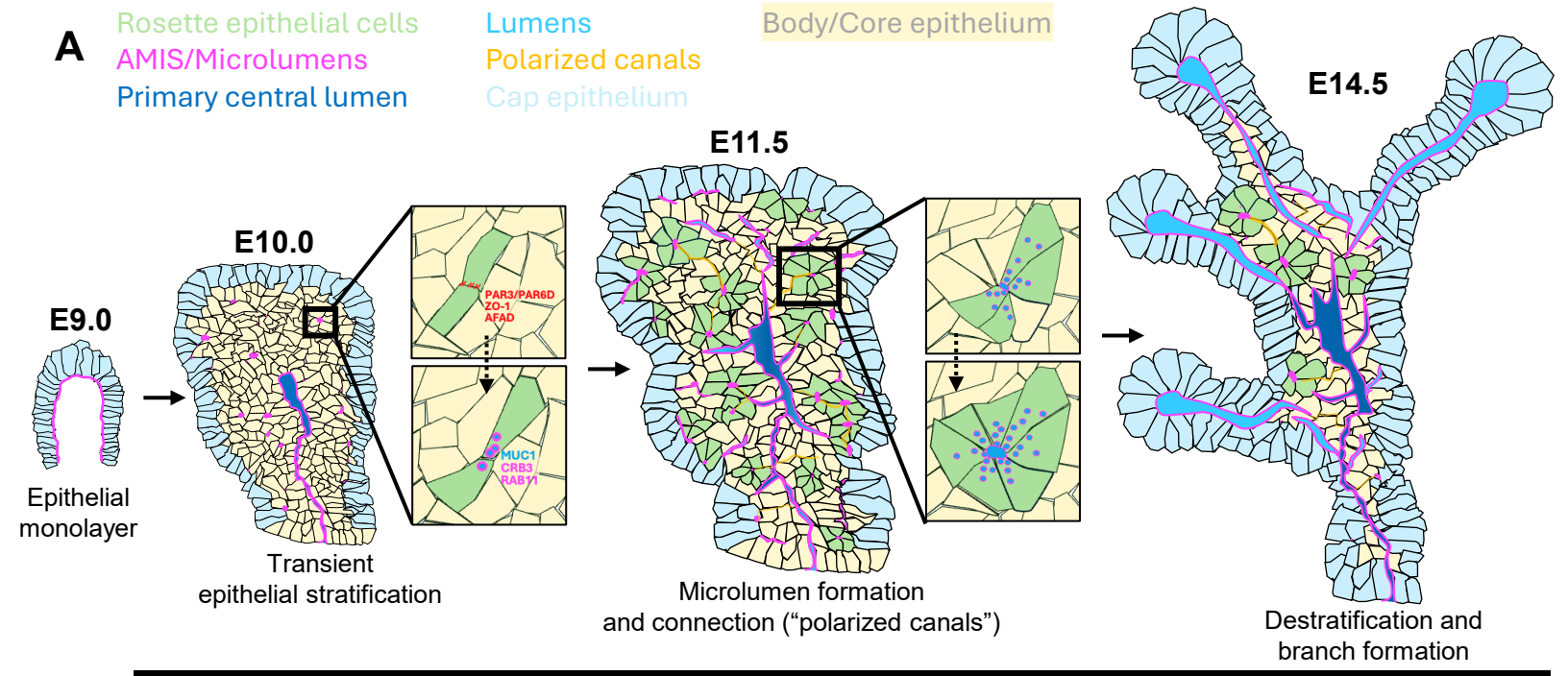

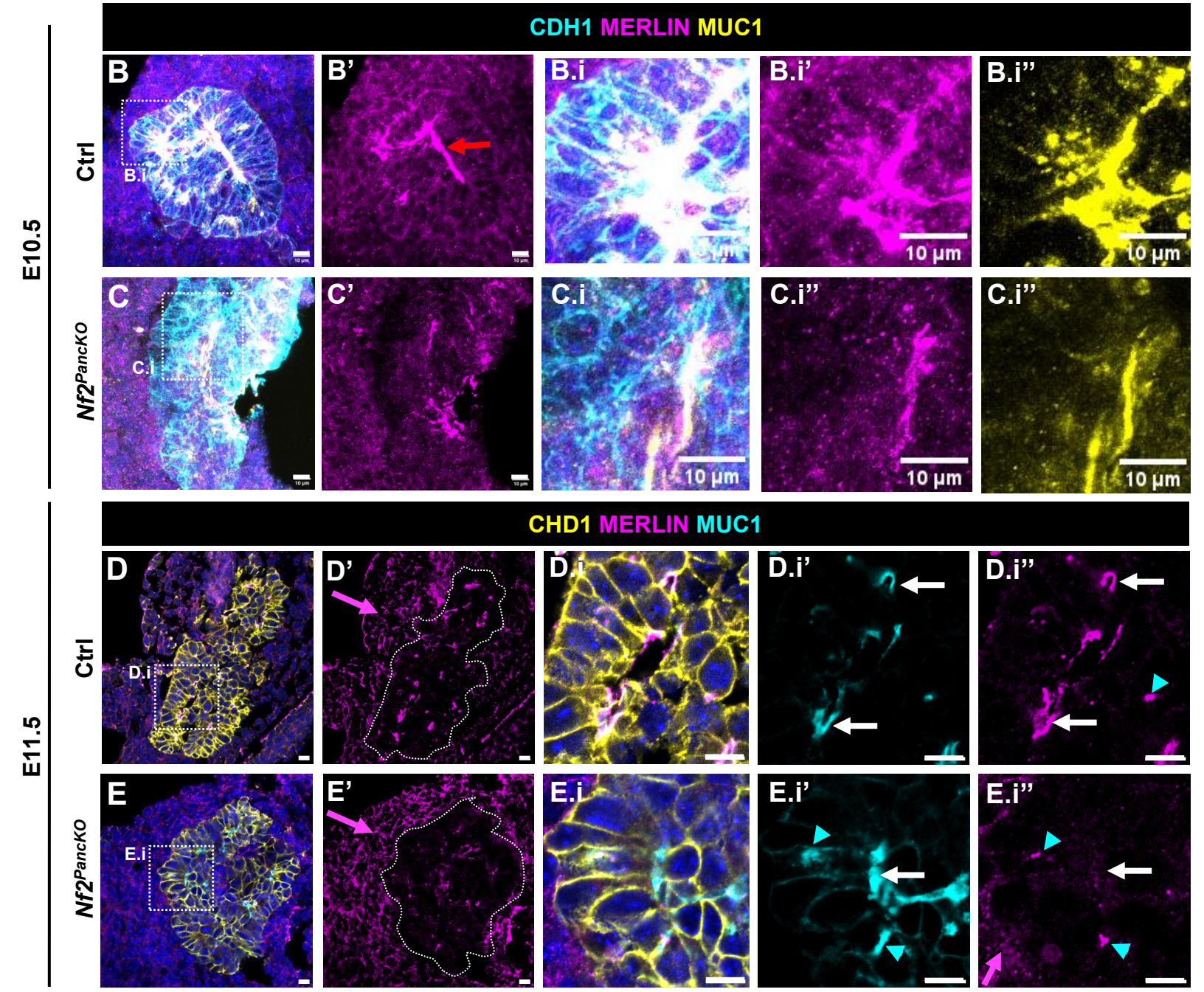

Fig. S3. Pdx1^{Cre} deletes MERLIN in pancreatic epithelium by E11.5, but not E10.5. **A**) Schematic of pancreatic morphogenesis depicting transient epithelial stratification followed by destratification, resolution, and branching. During destratification, *de novo* lumen formation is initiated as cells establish apical surfaces enriched in Par3, ZO-1, and AFA. These newly formed apical domains function as spatial landmarks that direct continued apical trafficking of proteins, including MUC1, thereby promoting lumen expansion and epithelial remodeling. IF for CDH1, MERLIN and MUC1 in E10.5 control **(B, B')** and *Nf2*^{PancKO} **(C, C')** pancreata (paraffin sections). Dotted lines in A' and B' outline the pancreatic epithelium. Red arrows indicate mesenchymal tissue. **B.i-C.i")** Higher magnification insets shown by boxed regions in B, C, respectively. IF for CDH1, MERLIN and MUC1 in E11.5 control **(D, D')** and *Nf2*^{PancKO} **(E, E')** pancreata (paraffin sections). Dotted line in D' and E' is tracing of CDH1, indicating pancreatic epithelium**. D.i-E.i")** Higher magnification insets shown by boxed regions in D, E, respectively. White arrows indicate lumens; cyan arrowheads, AMIS. Magenta arrowhead indicates mesenchymal tissue expressing MERLIN. All scale bars are 10mm.

Fig. S4. *Nf2*^{PancKO} E11.5 pancreatic explants exhibit defective epithelial remodeling and branching despite normal growth.

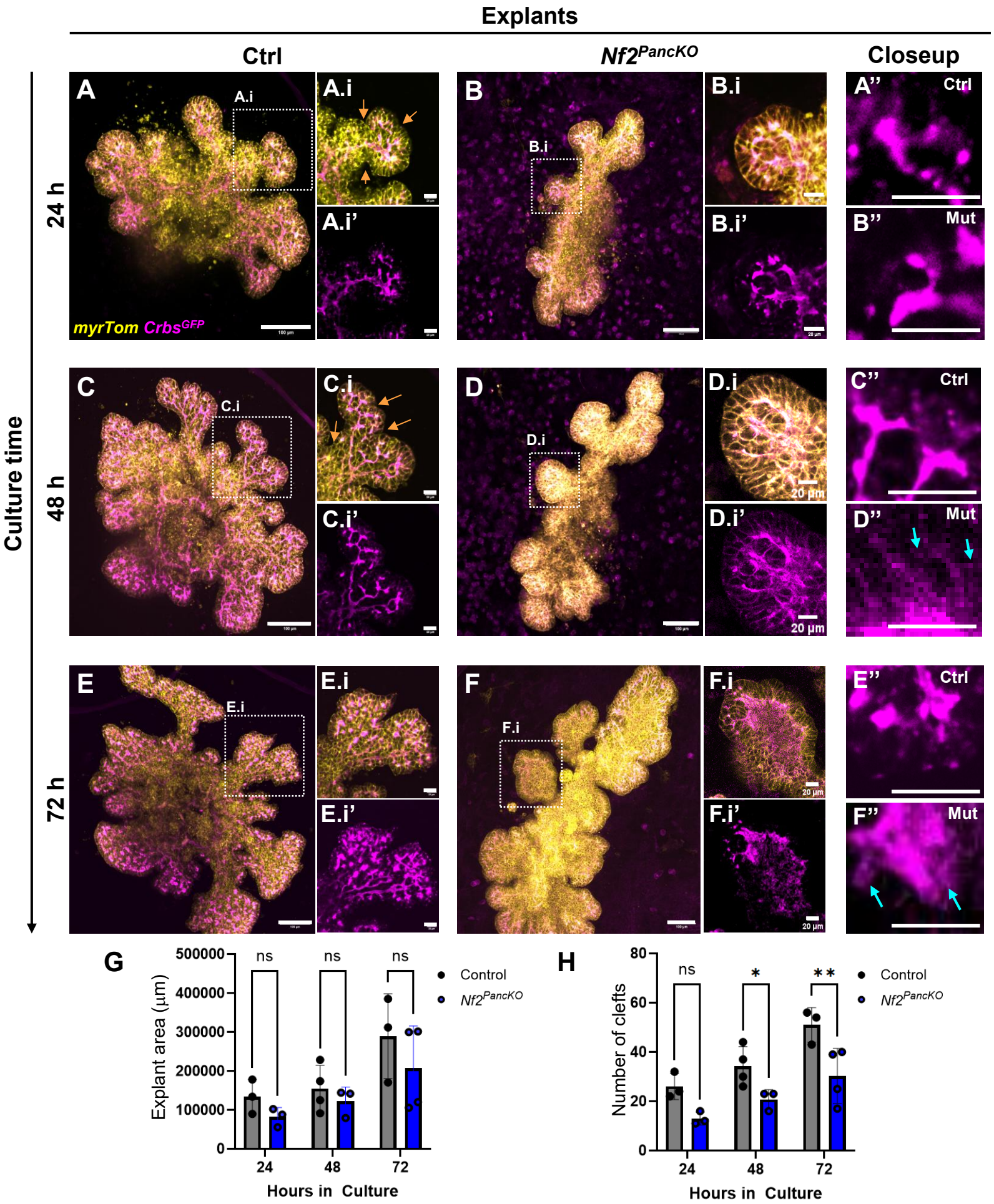

Fig. S4. *Nf2*^{PancKO} E11.5 pancreatic explants exhibit defective epithelial remodeling and branching despite normal growth. MIPs of control **(A,C,E)** and *Nf2*^{PancKO} **(B,D,F)** *myrTom;Crb3*^{GFP} explants at 24, 48 and 72 h of culture, respectively. **A.i-F.i')** Single optical sections corresponding to the regions outlined in white dashed boxes in A-F. *Crb3*^{GFP} single channel view of A'-F'. **A''-F'')** High magnification view of *Crb3*^{GFP} at 24-72 h of culture. Note accumulation of intracellular *Crb3*^{GFP} (blue arrows), and loss of branching clefts (orange arrows). **G)** Explant size was comparable between control and *Nf2*^{PancKO} cultures, through the 72-h imaging period (p=0.26, 0.39, 0.15 at 24, 48, and 72 h respectively, using two-way Anova with Tukey's multiple comparison test). **H)** *Nf2*^{PancKO} explants display defects in branching as measured by number of clefts (p=0.051, 0.038, 0.0070 at 24, 48, and 72 hours respectively, analyzed by 2-way Anova followed by Tukey's multiple comparison test). Scale bars: Panels A-F 100μm, and A.i-F'' 20μm.

Fig. S5. Loss of Merlin prevents epithelial destratification, blocking morphogenesis and proper cell fate allocation.

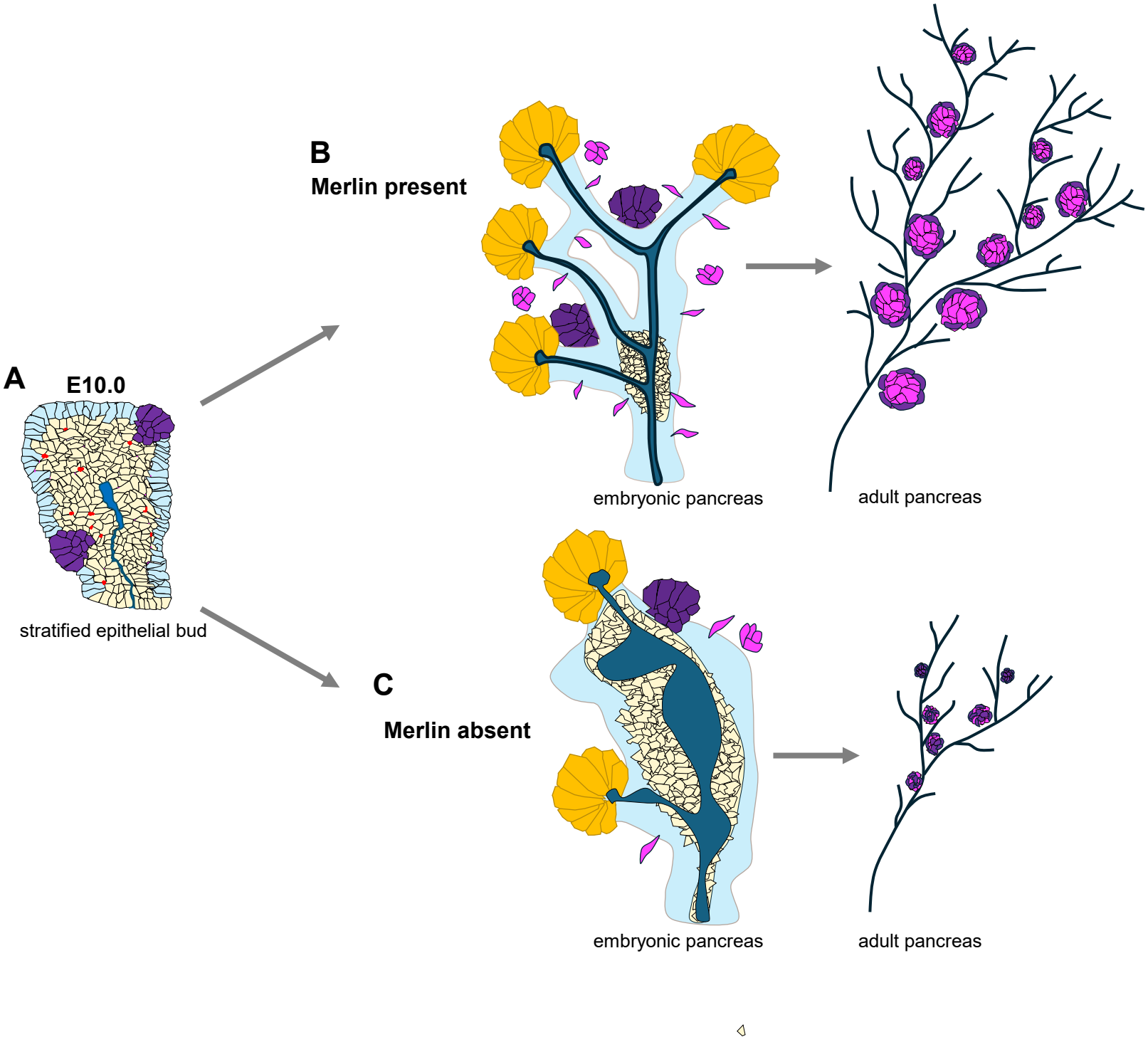

Fig. S5. Loss of Merlin prevents epithelial destratification, blocking morphogenesis and proper cell fate allocation. **A**) Pancreatic bud at E10.5 is composed of stratified epithelium (beige) and nascent microlumens (red), with the primary central lumen (dark blue) which is continuous with the gut tube lumen. Glucagon positive cells (purple) emerge in clusters at this early stage. **B)** When Merlin is present, the stratified epithelium of the embryonic pancreas resolves into monolayered epithelial tubes (pale blue) due to emergence and fusion of microlumens into a ductal plexus. Progenitors to endocrine cells reside solely within this transient plexus. Progenitors to all endocrine cells delaminate from the epithelial ductal tubes (magenta). At the tips of the plexus epithelial ducts, acini differentiate (orange). In the adult, the plexus is resolved and the pancreatic tree is a ramified gland, with large and small monolayered ducts, and large and small islets. Islets contain central insulin-expressing β-cells surrounded by a mantle of glucagon-expressing α-cells (purple). **C)** When Merlin is absent, enlarged lumens form, and the stratified epithelium fails to resolve. In the mutant adult, the overall pancreas is smaller with a reduction of endocrine mass and aberrantly composed islets.

Fig. S6. Cell polarity and AMIS components localize to nascent pancreatic microlumens.

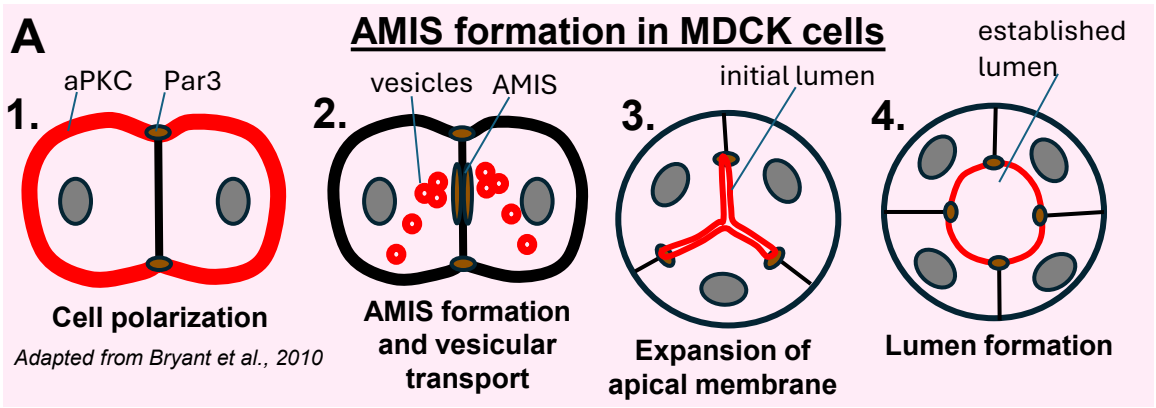

AMIS formation in pancreatic epithelial cells (E11.5)

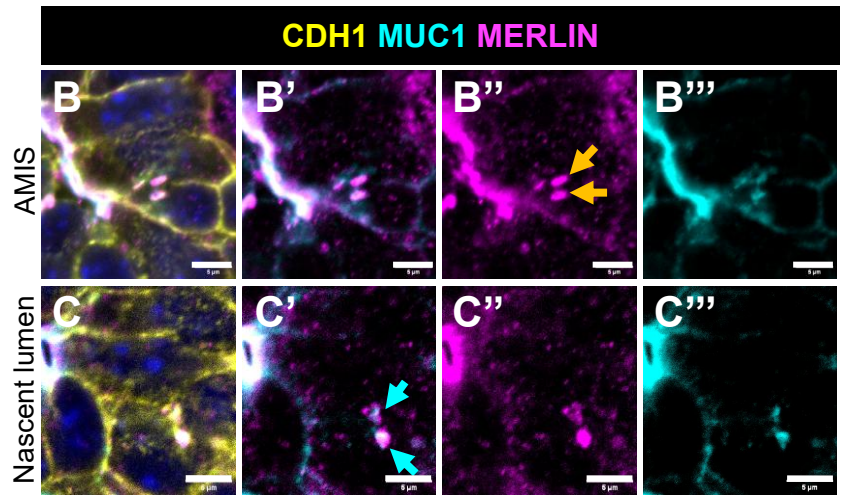

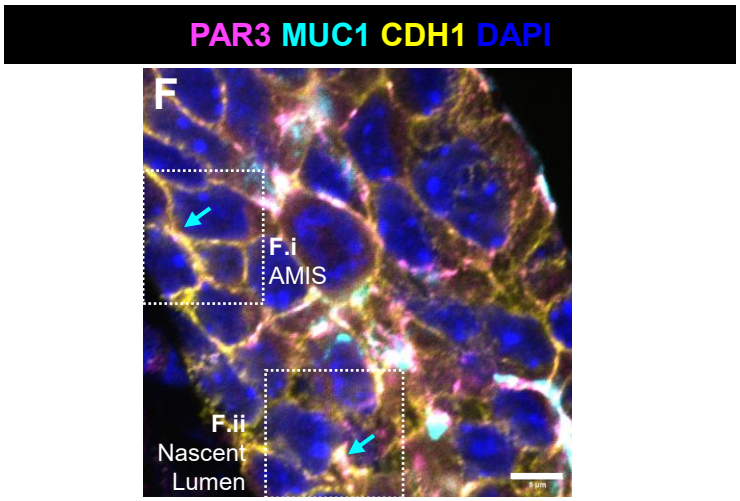

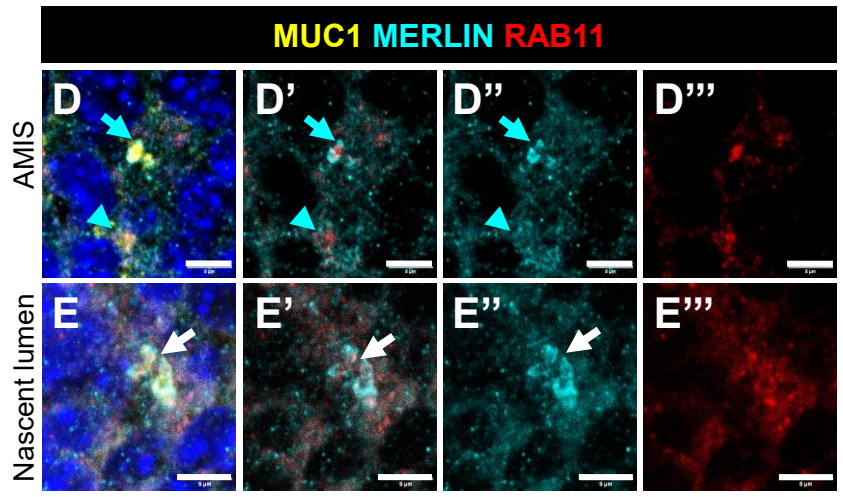

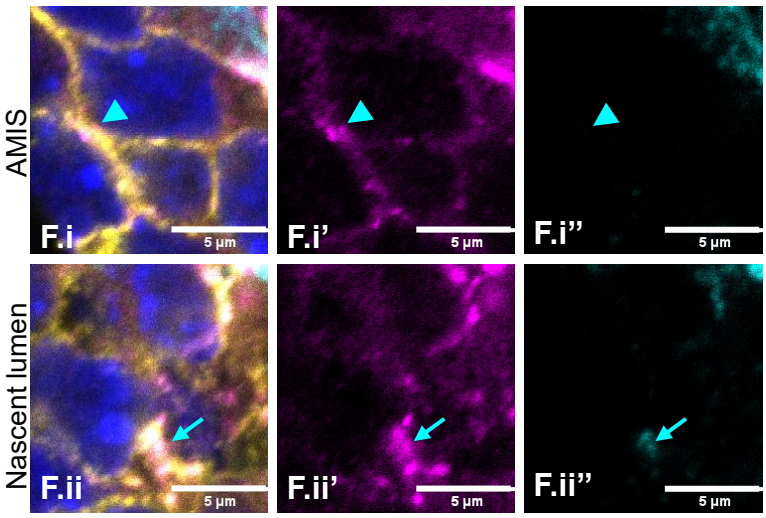

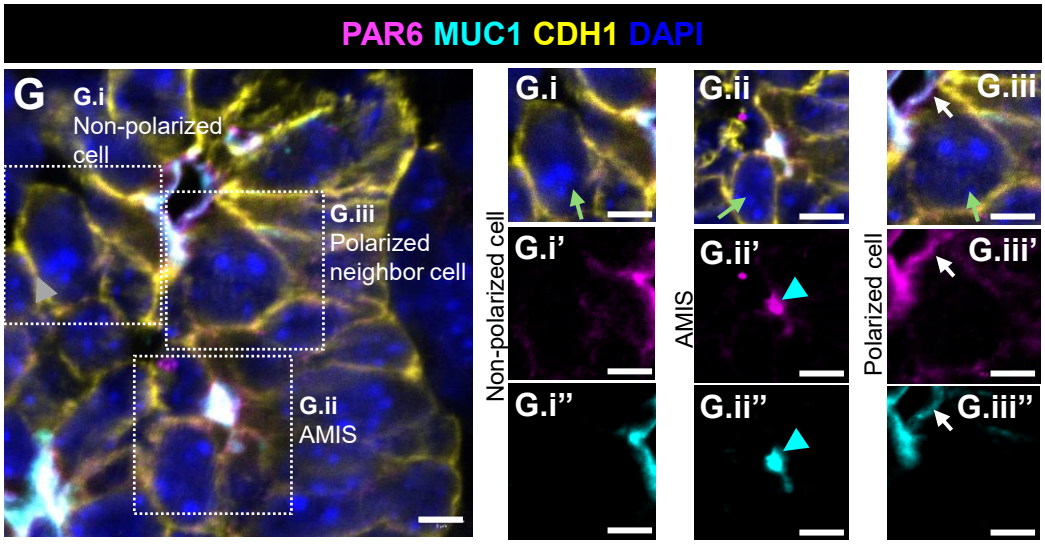

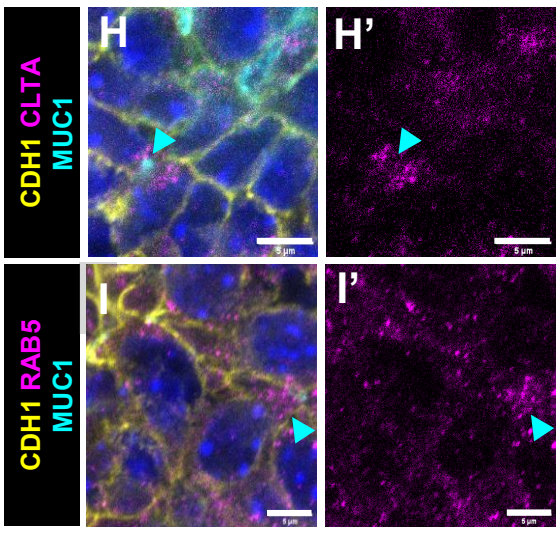

Fig. S6. Cell polarity and AMIS components localize to nascent pancreatic microlumens. **A)** Schematic of Apical Membrane Initiation Site (AMIS) formation based on studies in MDCK epithelial cysts, illustrating RAB11-dependent delivery of apical determinants including Crb3 and Par3 during *de novo* lumen formation. **B-C'")** MERLIN localizes to the subapical cortex of developing lumens and partially overlaps with MUC1 in E11.5 wild-type pancreatic epithelium. Orange arrows indicate intracellular MERLIN co-localizing with $MUC1^{+}$ vesicles. Blue arrowheads denote nascent lumens. **D-E'")** MERLIN and RAB11 localize to the AMIS, nascent lumens, and mature (open) lumens (cyan arrowhead, cyan arrow, and white arrow, respectively). **F)** IF for PAR3, MUC1 and CDH1 in wildtype E11.5 pancreas. **F.i-F.i")** PAR3 is enriched at cell-cell boundaries of developing lumens prior to detectable MUC1 accumulation, indicating the AMIS (cyan arrowheads). **F.ii-F.ii")** PAR3 remains enriched at the apical surface of nascent lumens $MUC1^{+}$ lumens (cyan arrows). **G)** IF for PAR6D, MUC1 and CDH1 in wildtype E11.5 pancreas. **G.i)** PAR6D is absent from stratified epithelial (SE) cells that have not initiated lumen formation. PAR6D becomes apically enriched at the AMIS (cyan arrowheads) **(G.ii),** and polarized lumen-lining cells (white arrows) **(G.iii)**. Green arrows, cells of interest. **H-I')** IF of wildtype E11.5 showing enrichment of CLTA and RAB5 at nascent lumens. All scale bars 5μm.

Fig. S7. Merlin is required to form the pancreatic AMIS and localize Par3.

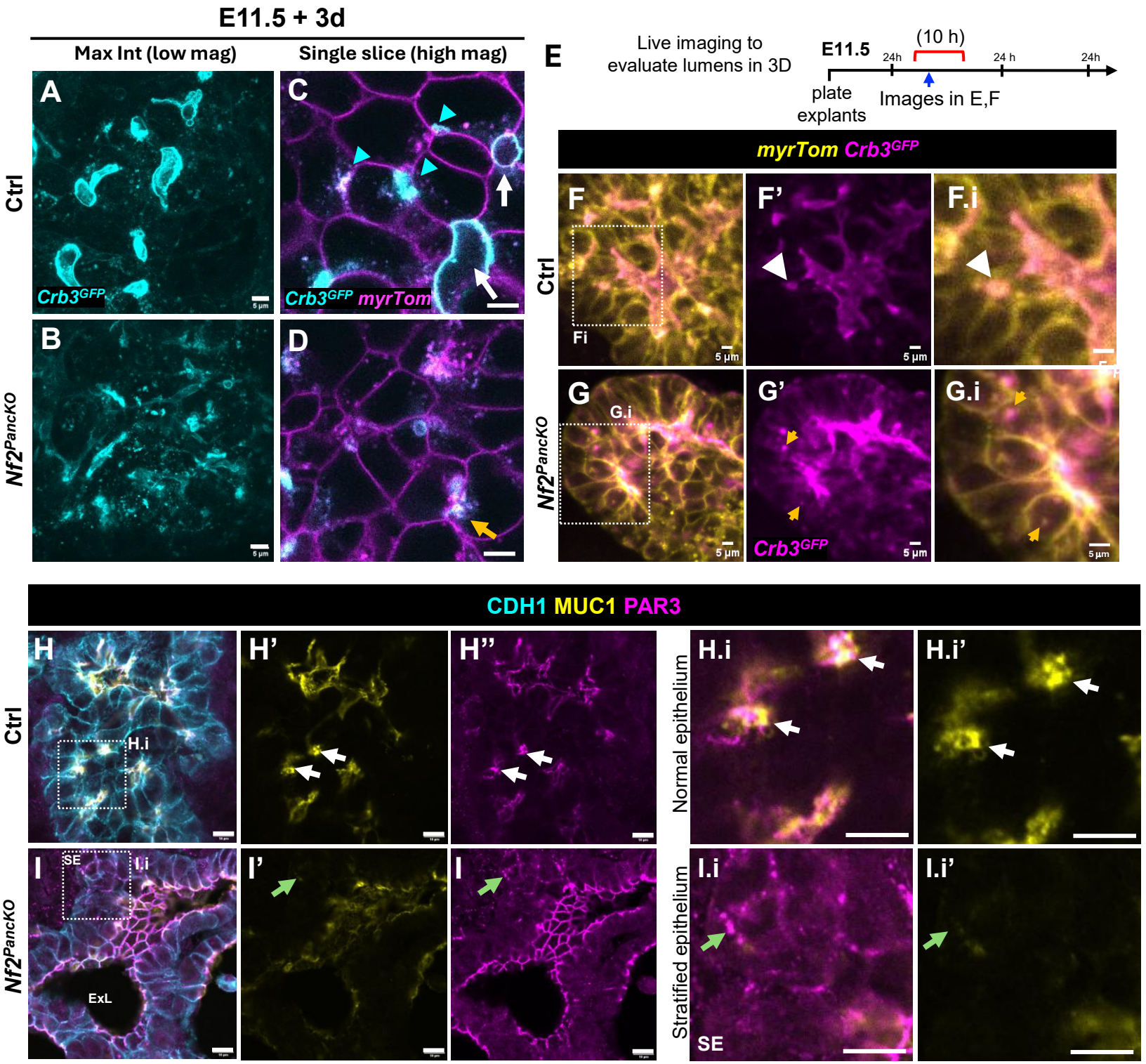

Fig. S7. Merlin is required for pancreatic AMIS formation and polarized localization of PAR3. MIPs of control **(A)** and mutant **(B)** explants at 3 days of culture. Images in B and C were taken from approximately 2 hours of live imaging time. Panels **C** and **D** are the same as Fig. 3G-H. MIPs of *Crb3*^{GFP} included here to provide context. **E)** Experimental schematic. Pancreata were explanted at E11.5 and live-imaged between 24-34 h of culture. **F)** In control epithelium, *Crb3*^{GFP} localizes exclusively between adjacent cells at nascent lumens (white arrowheads). **G)** In *Nf2*^{PancKO}, Crb3 accumulates in intracellular punctae, rather than at cell surfaces (orange arrows). **H)** In E14.5 control epithelium, PAR3 is tightly restricted to the apico-junctional region of lumen-lining cells (white arrows), co-localizing with MUC1. **I)** In stratified regions of *Nf2*^{PancKO}, PAR3 remains detectable (green arrows), but is dispersed along the cell cortex and is not associated with MUC1, indicating failure to assemble into discrete AMIS. Scale bars: Panels A-D and H-I.i' 10μm, F-G.i. 5μm.

Fig. S8. Epithelial phenotype summary: *De novo* lumens fail to form in *Nf2*^{PancKO}, while pre-existing lumens expand, likely due to dysregulated vesicular trafficking.

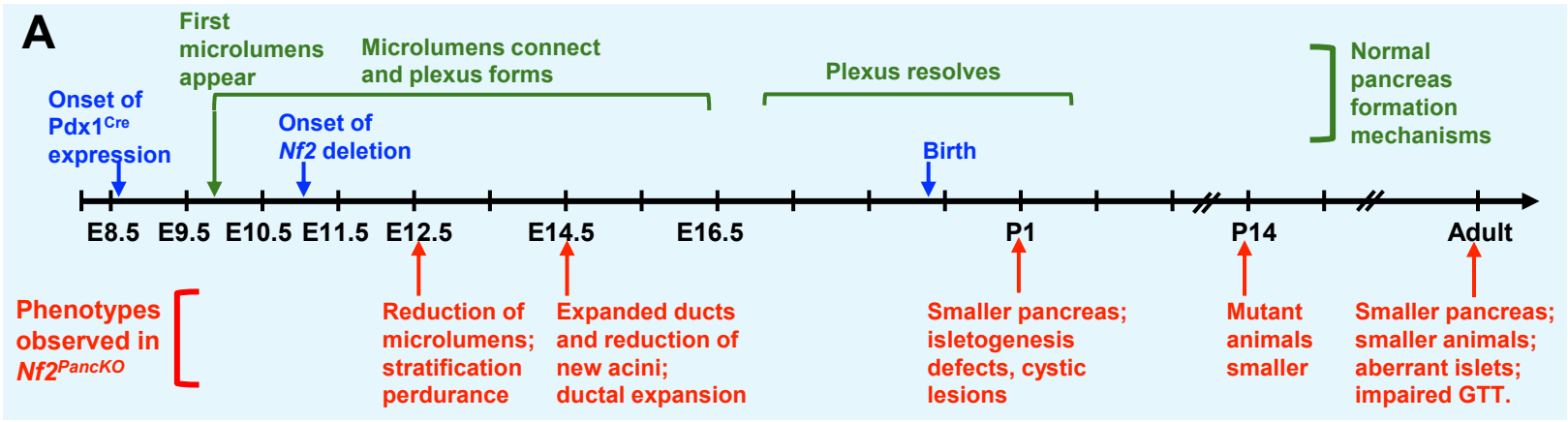

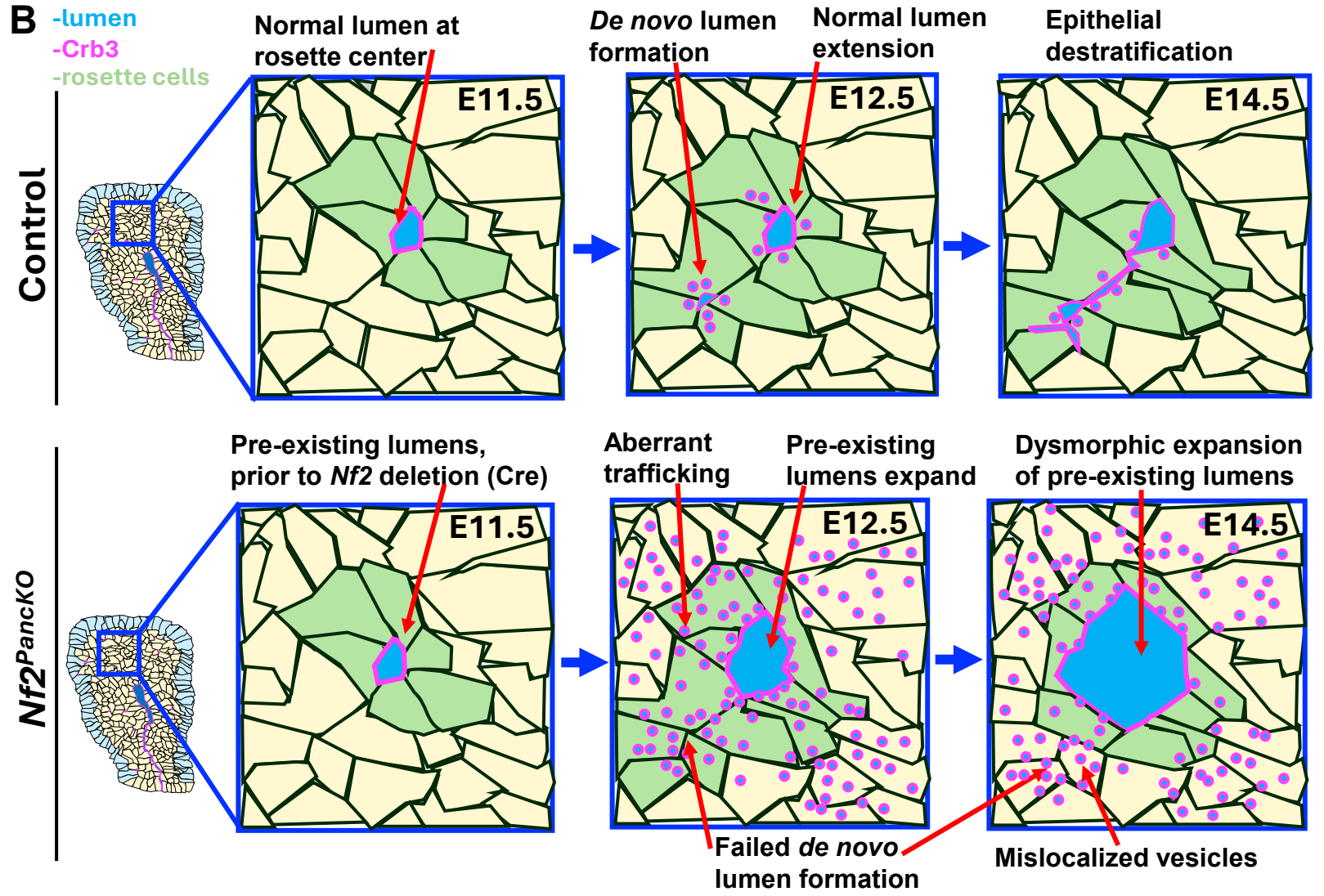

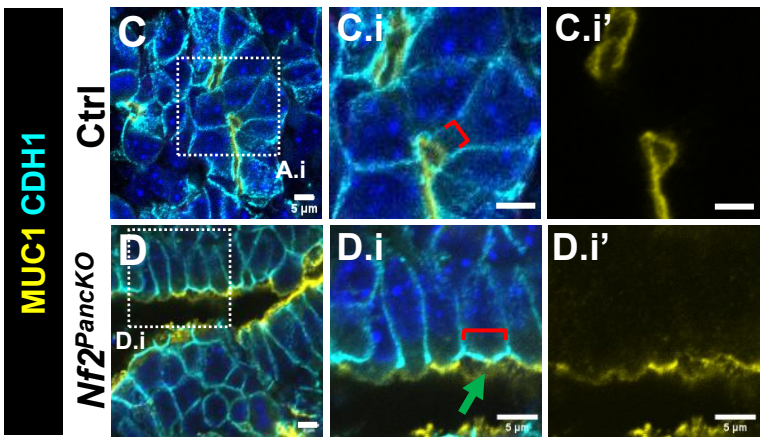

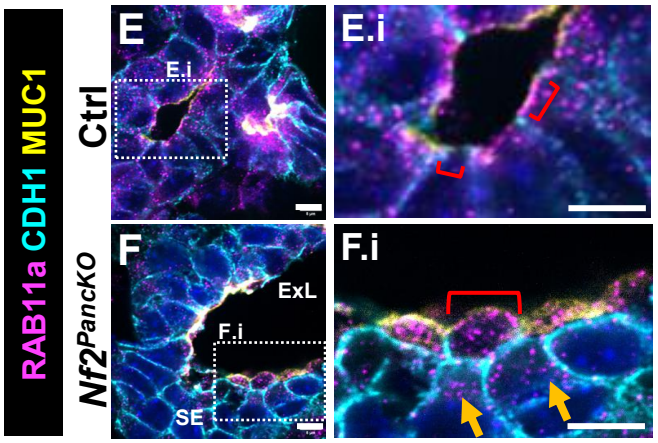

Fig. S8. Epithelial phenotype summary: *De novo* lumens fail to form in *Nf2*^{PancKO}, while pre-existing lumens expand, likely due to dysregulated vesicular trafficking. A) Timeline of phenotypes present in *Nf2*^{PancKO}. Pdx1^{Cre} expression begins at approximately E8.5, microlumen formation at approximately E10.0, and MERLIN deletion at approximately E11.5. First morphological defects are evident by E12.5. By E14.5, ductal defects are robust, and acinar numbers are reduced. By P1, pancreata are visibly smaller, and contain cystic lesions. Adult animals display reduced body size and impaired endocrine function. **B)** Models of epithelial processes in both control and mutant pancreata, between E11.5 and E14.5. In both genotypes, select cells have already undergone microlumen formation at E11.5. In controls, *de novo* lumens form, leading to lumen growth and epithelial destratification. In mutant pancreata, cells lining pre-existing lumens maintain polarity and continue to expand; however, cells that have not initiated lumens prior to Merlin deletion fail to assemble an AMIS and remain stratified. Mislocalization of vesicular trafficking components in these cells suggest that Merlin is essential for coordinating membrane trafficking during lumenogenesis. **C-D.i')** IF for CDH1 and MUC1 in control and mutant E14.5 tissue (15μm sections). In expanded lumens of mutant pancreata, the apical domain (red brackets) often appears expanded, and MUC1 extends into the lumens space along these rounded protrusions. Representative images are shown from >5 embryos per genotype. Rab11 IF on control **(E)** and mutant **(F)** pancreata at E14.5. Note accumulation of RAB11^{+} vesicles at the apical domain (red bracket) and increased cytosolic Rab11^{+} structures (orange arrows). All scale bars are 5μm.

Fig. S9. Persistence of partially polarized and apolar cells in E14.5 *Nf2*^{PancKO} pancreata.

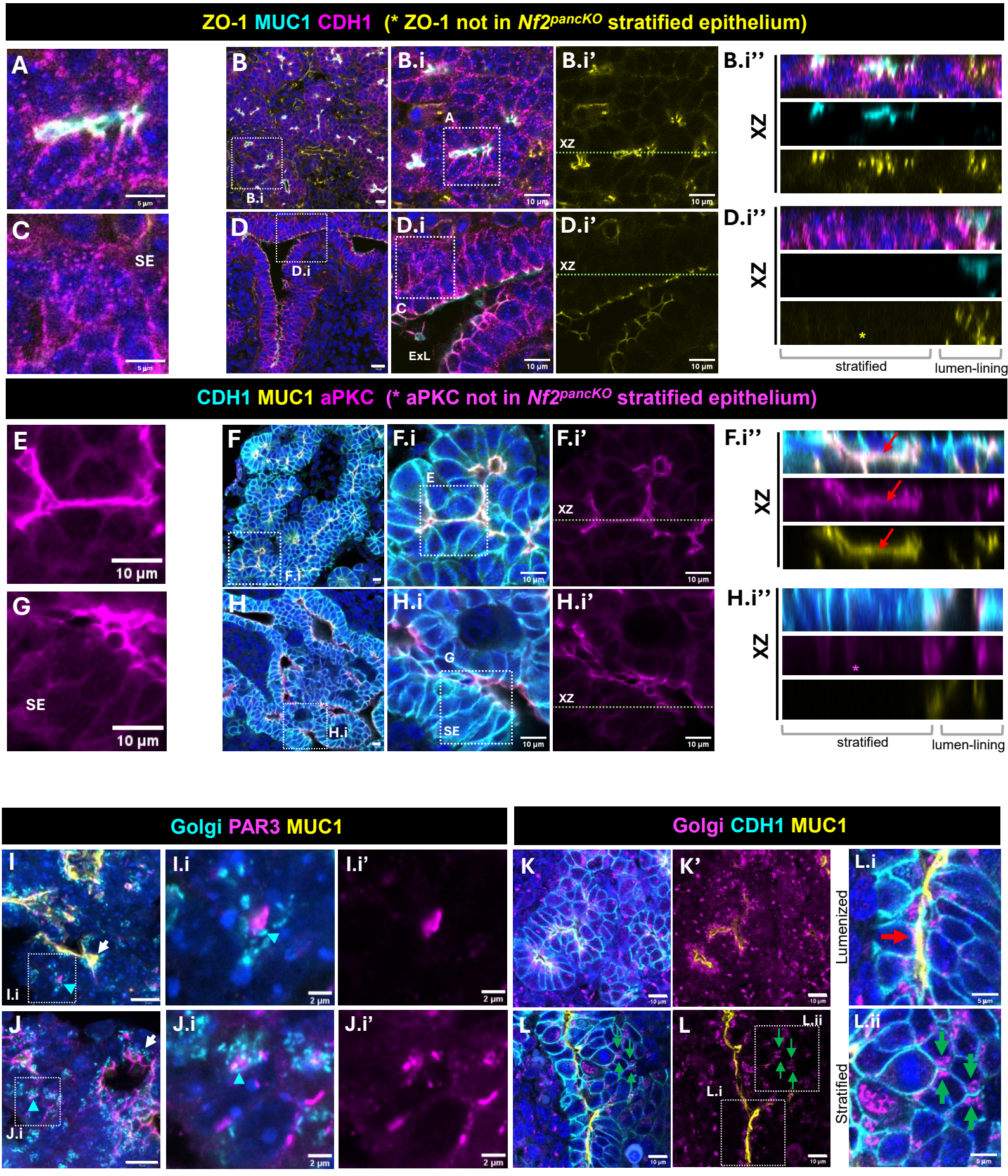

Fig. S9. Persistence of partially polarized and apolar cells in E14.5 *Nf2*^{PancKO} pancreata. A-D.i") Immunofluorescence (IF) for ZO-1, MUC1, and CDH1 in control and mutant pancreata. High-magnification views of central pancreatic epithelium in control **(A)** and mutant **(C)** tissue from panels B.i and D.i, respectively. SE indicates stratified epithelium. Dashed box indicates regions shown in B and D, respectively. **B.i-B.i")** ZO-1 is restricted to the apico-junctional regions of lumenized epithelium in control tissue. **D-D.i")** In mutant tissue, ZO-1 is correctly localized at expanded lumens, but is absent in stratified regions, in both XY plane and orthogonal (XZ) projections through the 10μm stack (**D.i").** Dashed green line in B.i' and D.i' indicates the planes used for orthogonal reconstructions. **E-H.i")** IF for aPKC, CDH1, and MUC1 in E14.5 control and mutant pancreata. aPKC is present at approximately the same levels in control and mutant tissue in lumen-lining cells. **E)** aPKC is tightly localized to the apical membrane in control tissue. **G)** In lumen lining cells of *Nf2*^{PancKO}, aPKC is present along the apical membrane. However, in SE regions, aPKC immunoreactivity was undetectable. Dashed green lines in F.i' and H.i' indicate plane used for orthogonal projections in **F.i"** and **H.i"**. **I-J.i')** IF for Golgi (GM130) and MUC1. In control pancreata (**I.i)**, the Golgi is localized subapically, under Par3, at both mature lumens (white arrow) and at developing AMIS (cyan arrowhead). In mutant AMIS **(J.i)**, Golgi positioning is maintained (cyan arrowhead), but no longer aligns with PAR3 localization at the AMIS. Golgi positions normally at expanded lumens (white arrow). **K-L.ii)** IF for Golgi (GM130), CDH1, and MUC1. **K, K')** In control pancreata, Golgi are localized to the subapical regions of lumen-lining epithelial cells (red arrow). **(L, L.i)** In *Nf2*^{PancKO}, lumen-lining cells display subapical Golgi, while stratified epithelial cells frequently oriend paired Golgi towards one another **(L.ii)**, indicating persistence of a polarized intracellular axis despite failure to establish an apical domain. For A-L, representative images from N $\geq$ 3 embryos evaluated per genotype. Scale bars are 10μm in all panels, except 5μm in A, C, L.i, L.ii and 2μm in I.i, I.i', J.i, J.i'.

Fig. S10. Loss of MERLIN disrupts the balance and spatial organization of RAB5⁺ and RAB11⁺ vesicle populations

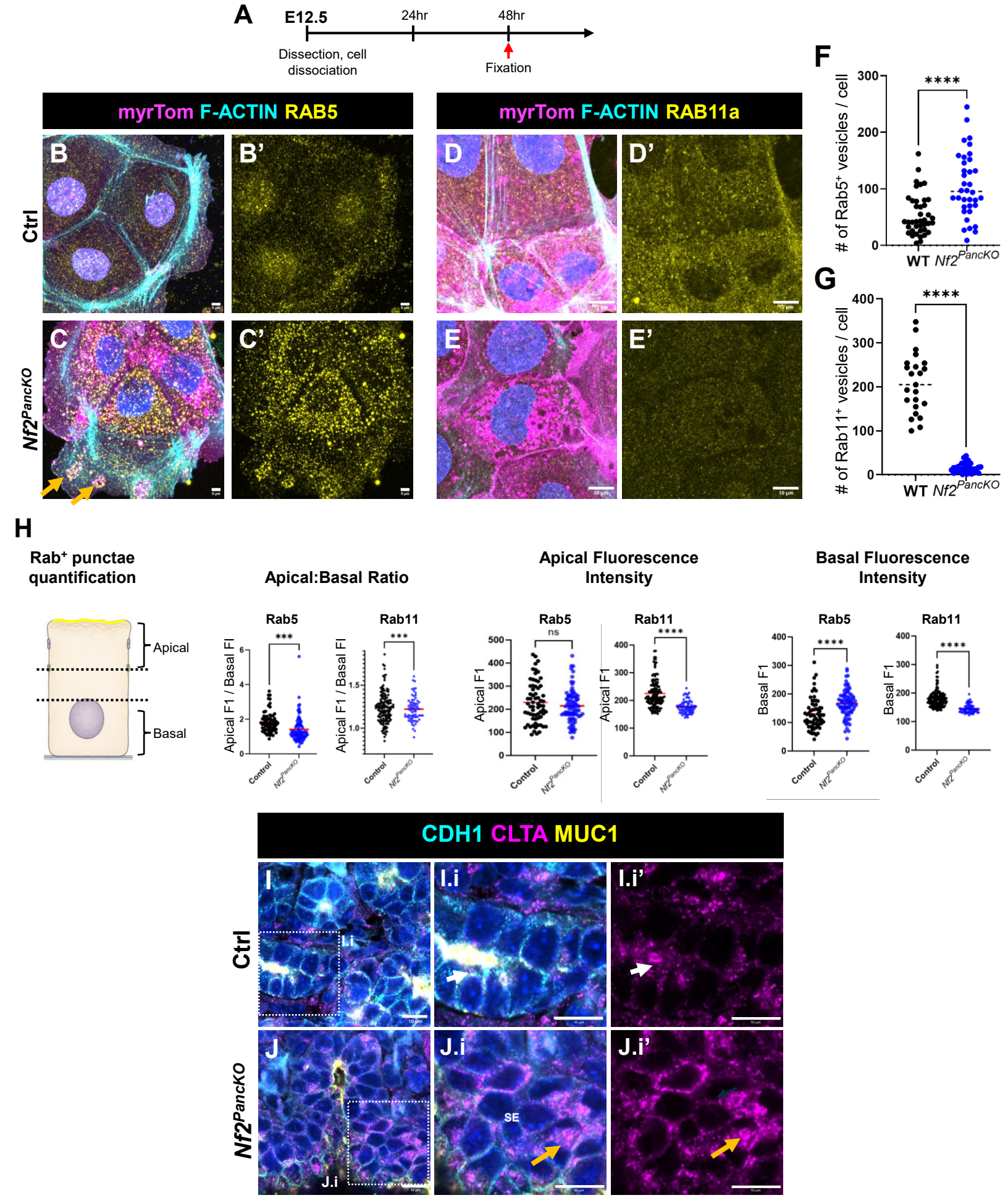

Fig. S10. Loss of MERLIN disrupts the balance and spatial organization of RAB5$^+$ and RAB11$^+$ vesicle populations. **A)** Experimental schematic for dissociated epithelial cell analysis. E12.5 pancreata were dissociated into single cells, cultured for 48 h, fixed, and processed for IF. **B-C')** IF for RAB5 in cultured control and *Nf2^{PancKO}* cells. Mutant cells exhibit increased numbers of RAB5$^+$ vesicles. Many intracellular myrTOM$^+$ structures are RAB5$^+$ (orange arrows). **D-E')** IF for RAB11 in cultured control and *Nf2^{PancKO}* cells. RAB11$^+$ vesicles are reduced in *Nf2^{PancKO}* cells. Quantification of number of Rab5$^+$ **(F)** and RAB11$^+$ **(G)** intracellular structures shows an overall increase of Rab5$^+$ and decrease of Rab11$^+$ vesicles. (For J, n= 40 control, and 36 mutant cells evaluated. P <0.0001 by Welch's t.test. For K, n=23 control and 35 mutant cells evaluated. P <0.0001 by Welch's t.test). **H)** Quantification of Rab5/Rab11 localization in lumen-lining MUC1$^+$ epithelial cells at E14.5. Cells were divided into apical and basal compartments, and fluorescence intensity (FI) was measured in each region. Note alteration of RAB5$^+$ and RAB11$^+$ vesicle distribution, with shift from Rab11-mediated recycling towards Rab5-endosomal compartments. (Mean gray value was utilized as a measure of FI for each portion of the cell. Data analyzed by Welch's t-test. P values = Rab5 Apical FI/Basal FI – 0.0001, Rab11 Apical FI/Basal FI – 0.0001, Rab5 Apical FI – 0.27, Rab11 Apical FI -- <0.0001, Rab5 Basal FI -- <0.0001, Rab11 Basal FI -- <0.0001). **I-J.i')** IF for clathrin heavy chain (CLTA) on control (I-I.i') and mutant (J-J.i') pancreata at E14.5. I) Normally, CTLA accumulated at forming lumens that express MUC1. J) In mutant epithelia, CTLA is ectopically localized in the cytoplasm (orange arrows), consistent with disrupted membrane trafficking. Scale bars: Panels B-C' 5μm, D-E' and I –J.i' 10μm. For all graphs, midline represents median.

Fig. S11. Loss of MERLIN preferentially disrupts trafficking protein localization in the core stratified epithelium.

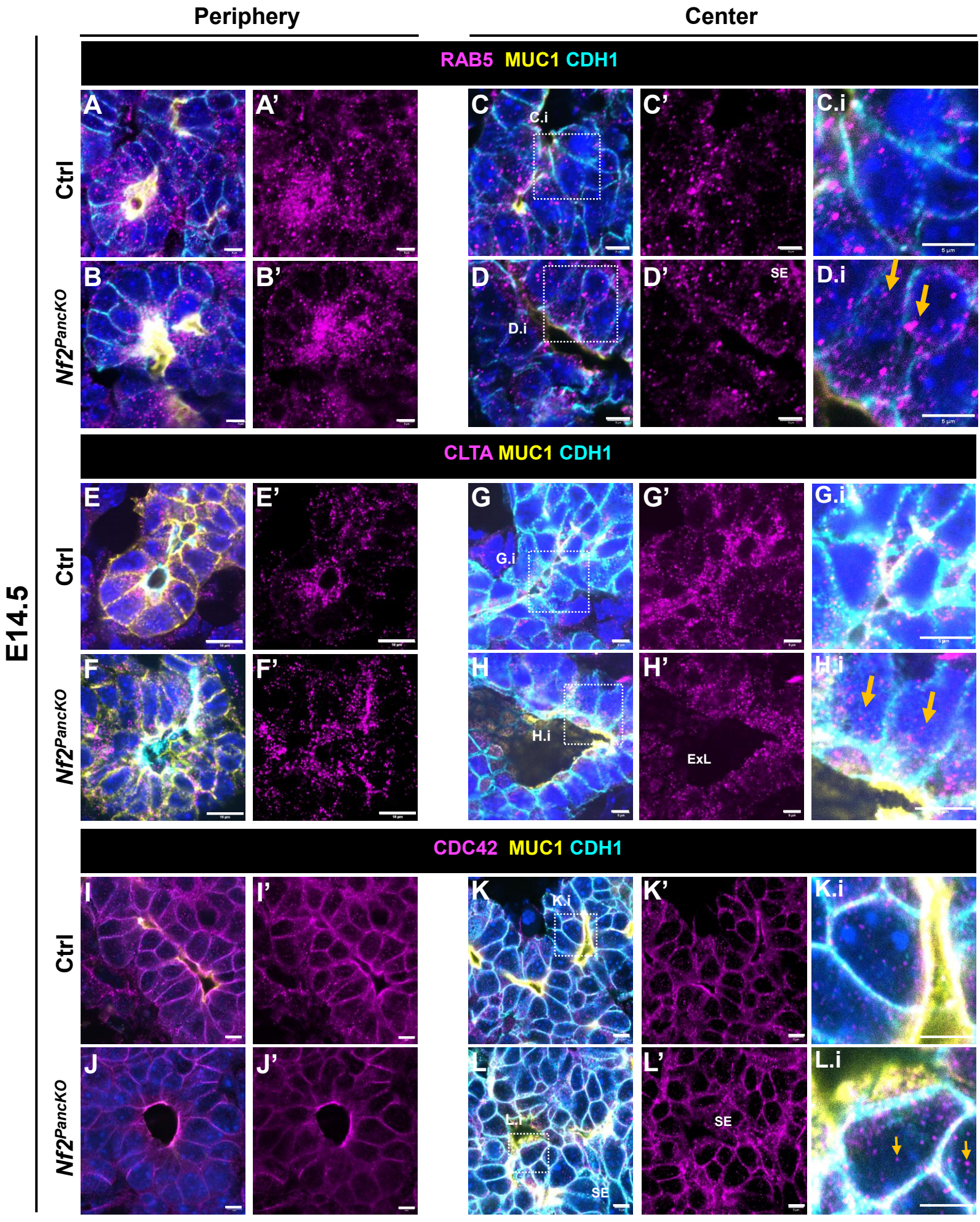

Fig. S11. Loss of MERLIN preferentially disrupts trafficking protein localization in the core stratified epithelium. A-L.i') IF for trafficking components in E14.5 control and *Nf2*^{PancKO} pancreata. Peripheral (A-B', E-F', J-K') and central (C-D.i, G-H.i, L-M.i) epithelial regions are shown. **A-D.i)** IF for RAB5 in E14.5 control (A, C) and *Nf2*^{PancKO} (B, D) pancreata. **C.i, D.i)** Dotted lines indicate region of high magnification views. RAB5 is enriched along the MUC1^{+} apical membrane, particularly in peripheral epithelium of both control and mutant cells, but accumulates in ectopic cytoplasmic punctae in the core epithelium of mutants (orange arrows). **E-H.i)** IF for CTLA in E14.5 control (E, G) and *Nf2*^{PancKO} (F, H) pancreata. **G.i, H.i)** High magnification views. CTLA is apically localized in both control and mutant tissue, but shows increased cytoplasmic localization in mutant cells (orange arrows). **I-L.i)** IF for CDC42 in E14.5 control (I, K) and *Nf2*^{PancKO} (J, L) pancreata. **K.i, L.i)** High magnification views. CDC42 is enriched along the MUC1^{+} apical membrane, in both controls and mutant cells, exhibits increased cytoplasmic localization in core epithelial mutant cells. In all three cases, trafficking defects are more pronounced in the central (core) region of the pancreas. MERLIN-dependent trafficking defects first appear in the epithelial population that fails to form new lumens following Cre-mediated deletion. Representative images from N $\geq$ 2 embryos evaluated per genotype. Scale bars: Panels A-D.i, G-L.i' 5μm, and E-F' 10μm.

Fig. S12. Loss of MERLIN alters lineage composition at E14.5.

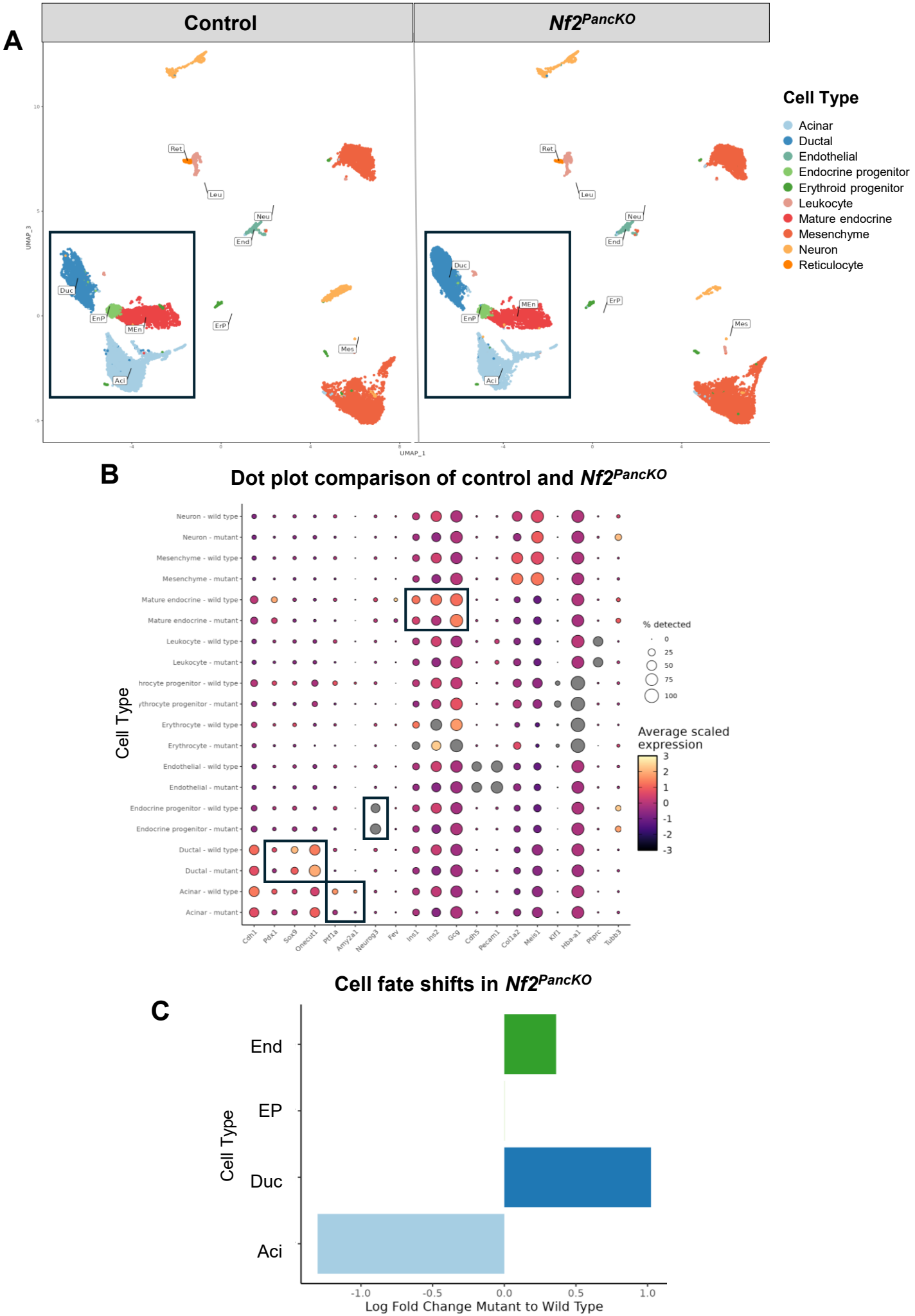

Fig. S12. Loss of MERLIN alters lineage composition at E14.5. Transcriptomic comparison of control and *Nf2*^{PancKO} epithelium at E14.5, using only E14.5 dataset. **A)** UMAP representation of single nuclear sequencing (snRNA-seq) from E14.5 control and mutant pancreata. Boxes highlight the major epithelial populations. A total of 11,511 epithelial nuclei were analyzed from control pancreata, and 8,020 epithelial nuclei were obtained from *Nf2*^{PancKO}. Acinar, ductal, endocrine progenitor, and endocrine clusters were identified. **B)** Canonical marker genes were used to identify epithelial cell populations and for cluster annotations. Black boxes denote markers of interest. **C)** Relative abundance of epithelial cell populations in control and mutant pancreata. Loss of MERLIN results in expansion of ductal cells, a modest increase in endocrine cells, and a corresponding reduction in acinar cells. Control epithelial nuclei contained: acini – 49%, ductal --26% endocrine progenitor – 14%, endocrine – 7%; whereas *Nf2*^{PancKO} epithelial nuclei contained: acini –20.4%, ductal –50.2% endocrine progenitor – 14%, endocrine – 12%.

Fig. S13. Transcriptomic analysis of control embryonic pancreas using integrated datasets from E11.5 and E14.5.

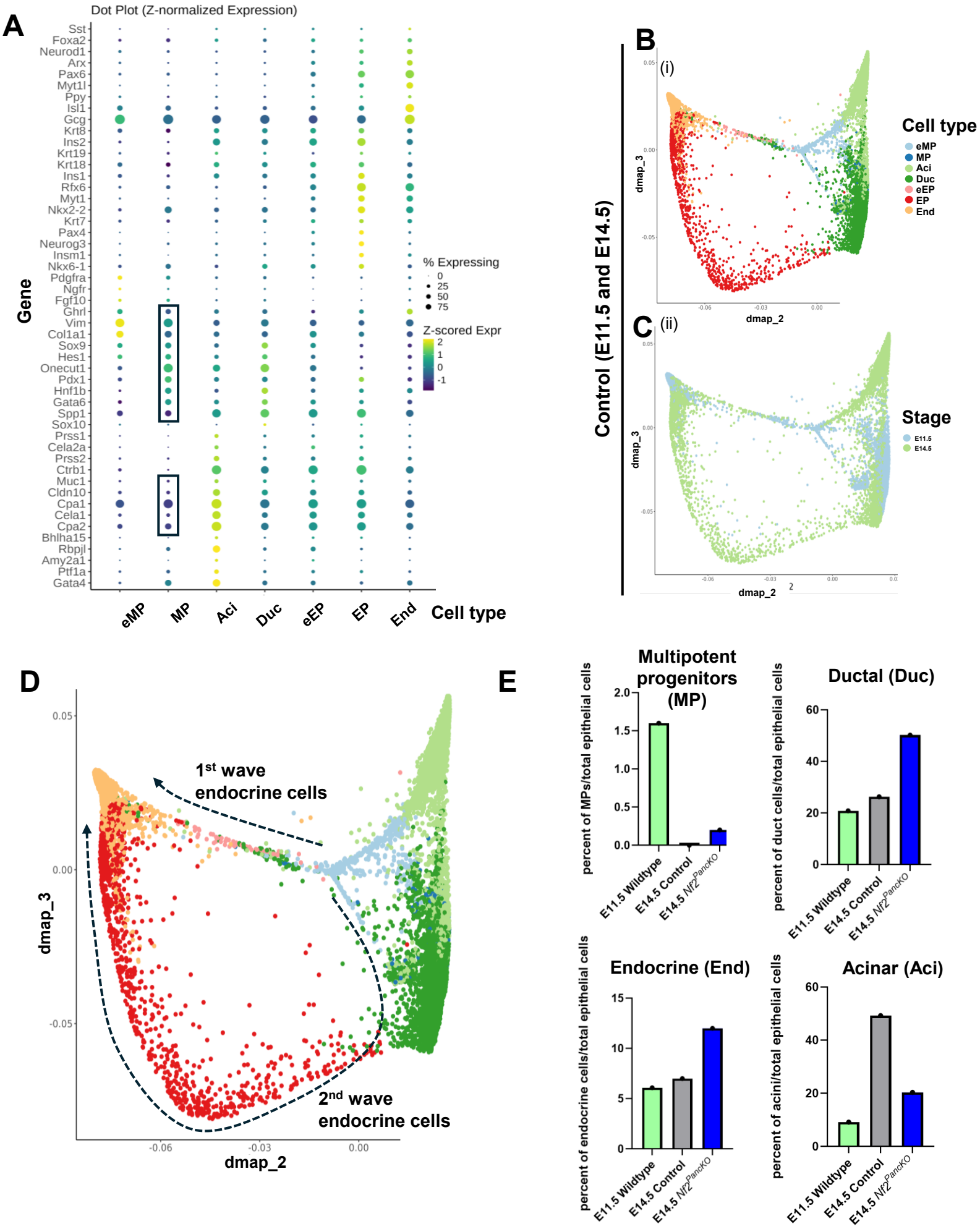

Fig. S13. Transcriptomic analysis of control embryonic pancreas using integrated datasets from E11.5 and E14.5. A) Markers used to assign cluster IDs are of integrated E11.5 and E14.5 data. **B)** Diffusion map of combined control E11.5 and E14.5 data. **C)** E11.5 cells are shown in light blue, and E14.5 cells are shown in green. **D)** 1st and 2nd wave endocrine cells are annotated. First wave endocrine cells are on the arm which is composed of E11.5 and E14.5 cells, while the second wave endocrine cells are on the arm which is predominately E14.5 cells. E) Percentage of epithelial cells assigned to each selected cell type across conditions.

Fig. S14. Integration of E11.5 and E14.5 data sets.

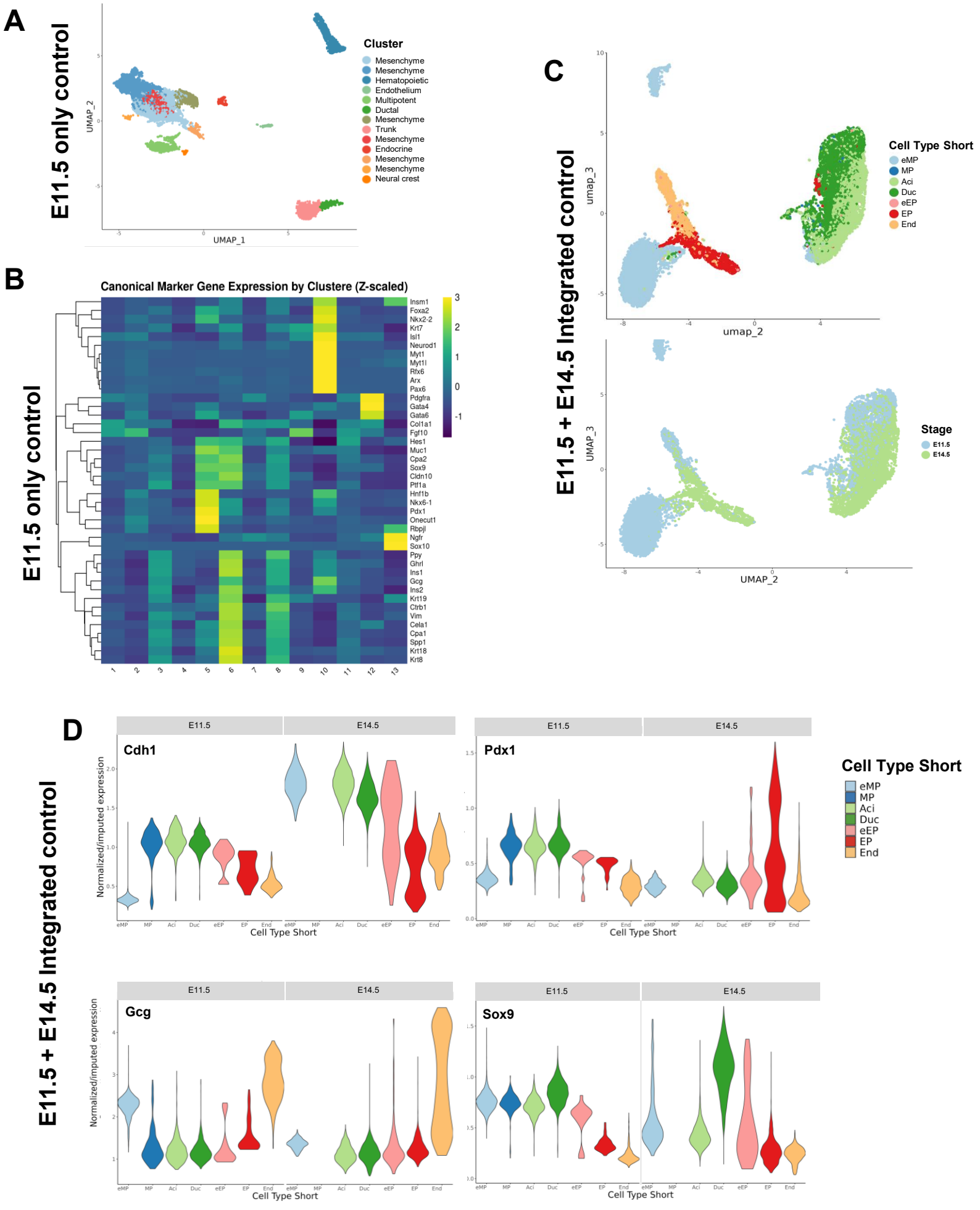

Fig. S14. Integration of E11.5 and E14.5 data sets. A) UMAP of E11.5 wildtype pancreata – 12,834 epithelial cells from E11.5 pancreata were obtained. **B)** Markers used to assign cluster IDs are of integrated E11.5 data **C)** Umap of combined control E11.5 and E14.5 data. **C')** E11.5 cells are shown in light blue, and E14.5 cells are shown in green. **D)** Expression of key marker genes in integrated data set, with clusters split by stage.

Fig. S15. Endocrine mass transiently increases in *Nf2*^{PancKO}, but subsequent isletogenesis is disrupted and postnatal endocrine mass is reduced.

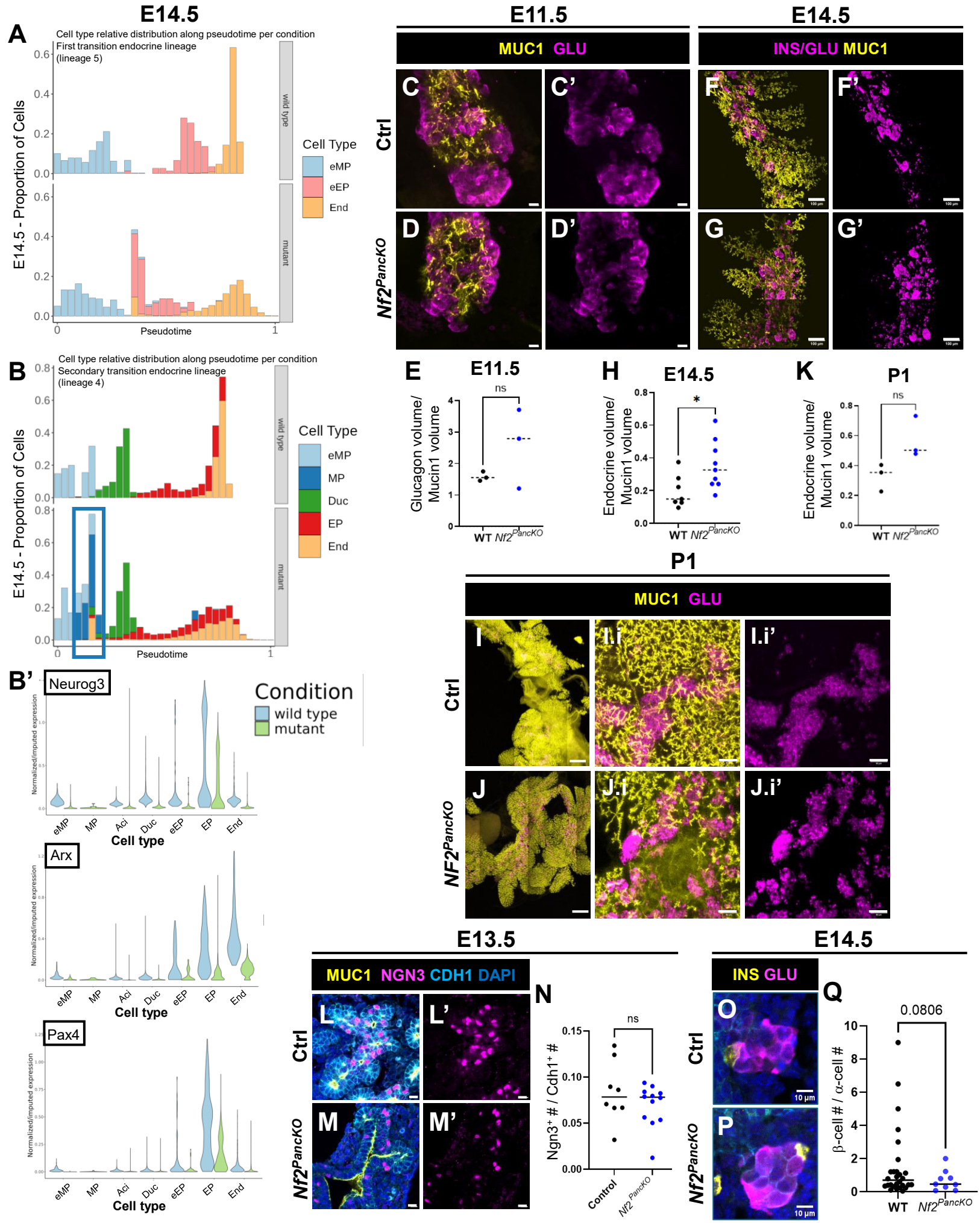

Fig. S15. Endocrine differentiation is delayed in *Nf2*^{PancKO} pancreata, resulting in reduced postnatal endocrine mass. Endocrine mass transiently increases in *Nf2*^{PancKO}, and subsequent isletogenesis is disrupted. **A, B)** Pseudotime distributions (histograms) of cells progressing along the early (A) and late (B) endocrine differentiation trajectories reconstructed from combined E11.5 and E14.5 single nucleus RNA-seq datasets. Mutant pancreas exhibit delayed progression along both endocrine trajectories. **B')** Expression of key endocrine differentiation markers (*Neurog3, Arx, and Pax4*) in from E14.5 data using clustering from combined E11.5 and E14.5 datasets. **C-J.i')** WMIF of control **(C, F, I)** and *Nf2*^{PancKO} **(D, G, J)** pancreata at E11.5 **(C, D)**, E14.5 **(F, G)**, and P1 **(I-J.i**') for MUC1 and GLU **(C, D)**, INS/GLU and MUC1 **(F, G)** and MUC1 and GLU **(I, J)**. E11.5 pancreata is stained for MUC1 and glucagon only, for other time points pancreata are stained for MUC1 and combined antibodies against insulin and glucagon. **E,H,K)** Quantification of endocrine volume at E11.5 **(E)**, E14.5 **(H)**, and P1 **(K)**, respectively. Each dot represents an individual animal analyzed. (P= 0.25, 0.02, 0.06 by unpaired t.test, respectively). Section IF of E13.5 control **(L, L')** and *Nf2*^{PancKO} **(M, M')** for MUC1, NGN3, and CDH1 at E13.5 . **N)** Quantification of NGN3+ cells shows no significant difference between genotypes (p=0.26 n=3 ctrl, 3 mutant animals analyzed). **O-Q)** Section IF for insulin and glucagon in E14.5 control (O) and mutant (P) pancreata. **Q)** Quantification of the ratio of β-cells:α-cells at E14.5 shows no significant difference between genotypes (p=0.08 by Welch' t-test, n=4 mutants, 6 ctrl animals evaluated). Each dot represents one FOV. Scale bars: Panels C-D' 10μm; F-G' 100μm; I-J 250 μm; I.i-J.i' 50μm' L-M' 10μm, O, P 10μm. For all graphs, midline indicates median.

Fig. S16. Acinar cells are poorly differentiated in *Nf2*^{PancKO}.

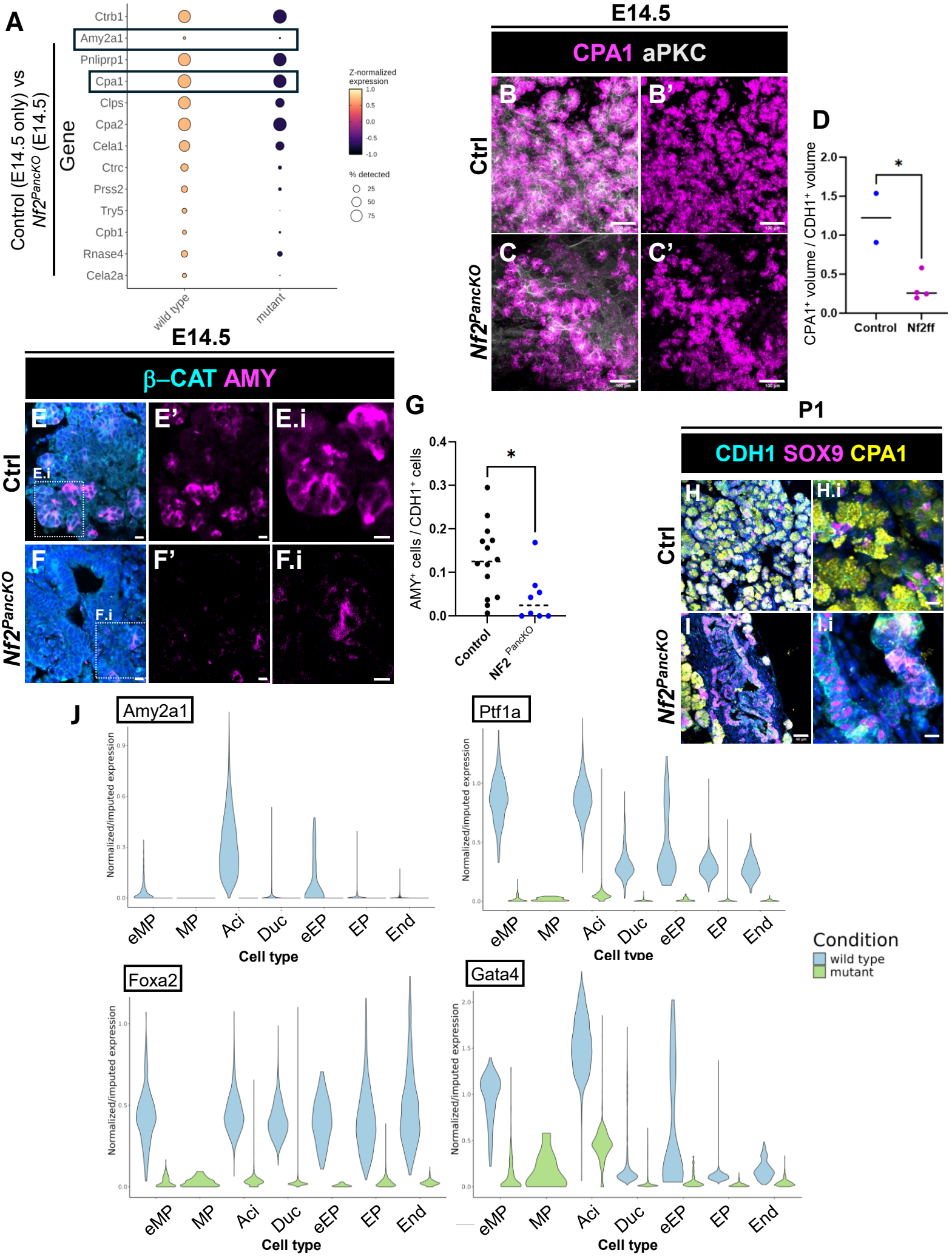

Fig. S16. Acinar cells are poorly differentiated in *Nf2*^{PancKO}. **A)** Dot plot showing reduced expression of key acinar secretory genes from E14.5 mutant acinar nuclei relative to E14.5 controls, using the clustering from the integrated single nucleus dataset. WMIF of E14.5 control **(B, B')** and *Nf2*^{PancKO} **(C, C')** pancreata stained for aPKC and CPA1. **D)** Quantification of CPA1^{+} volume. Each dot represents one pancreas, p = 0.018 by unpaired t-test. Section IF of E14.5 control **(E-E.i)** and *Nf2*^{PancKO} **(F-F.i)** stained for β-catenin (β-CAT) and amylase (AMY). White boxes indicate region magnified in **E.i-F.i. G)** Quantification of AMY^{+} epithelial cells per FOV. Each dot represents a single FOV analyzed, from n = 3 ctrl and mutant pancreata each. AMY^{+} epithelial cells are reduced in *Nf2*^{PancKO}. P =0.0044 by unpaired t-test. **H-I.i)** IF of control (H) and mutant (I) pancreata for CDH1, SOX9, and CPA1 at P1. **J)** Violin plots of *Amy2a*, *Ptf1a*, *Foxa2*, and *Gata4* from integrated dataset, comparing E14.5 control and mutant nuclei. Scale bars: Panels B-C' 100μm; E-F.i, H.i, I.i 10μm; and H,I 50μm. For D-G, midline indicates median.

Fig. S17. MERLIN is required during pancreatic lineage establishment but not lineage maintenance.

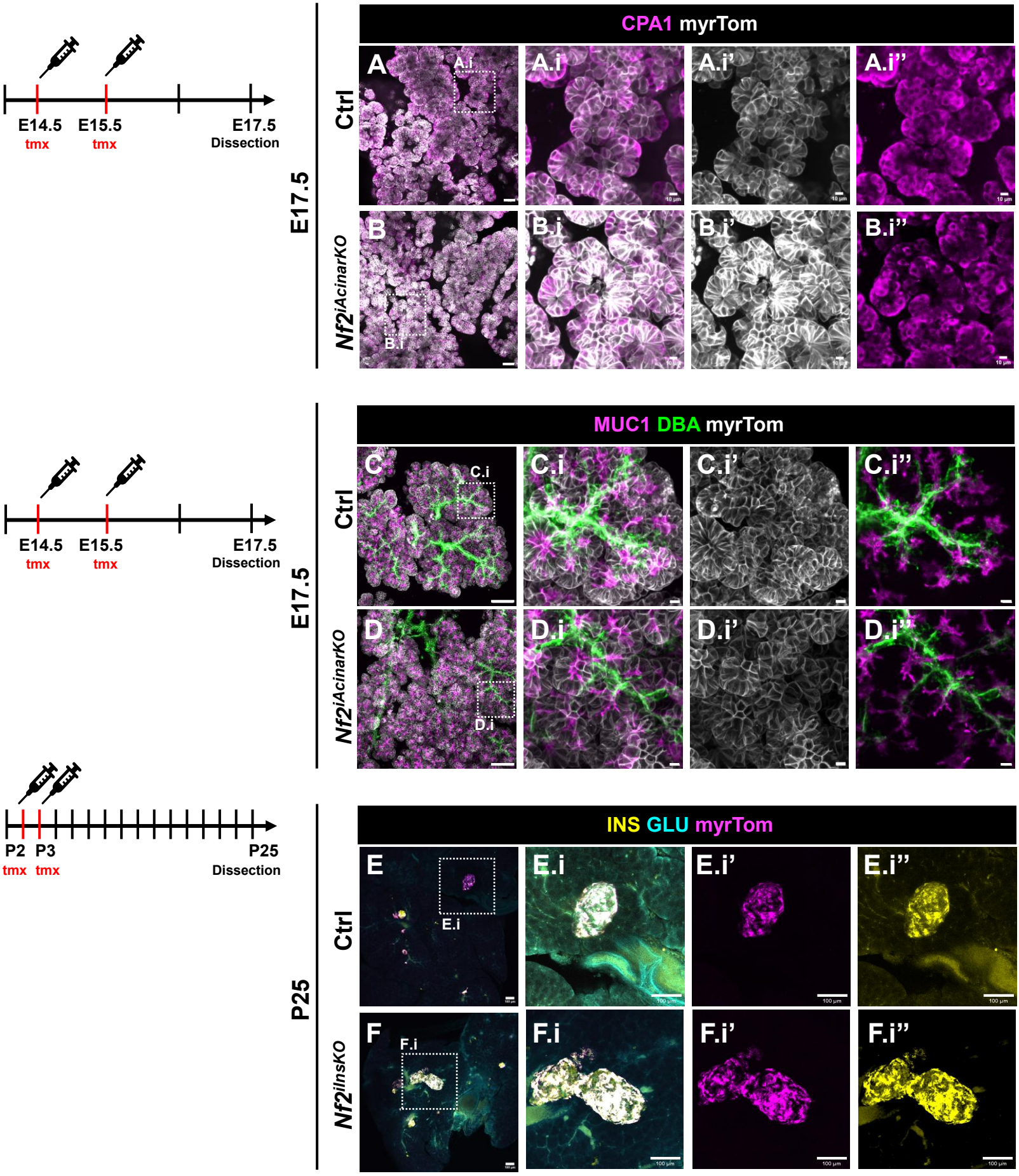

Fig. S17. MERLIN is required during pancreatic lineage establishment but not lineage maintenance. A-B.i") Representative 200μm vibratome section of E17.5 control (A) and *Nf2*^{iAcinarKO} (B) pancreata stained for CPA1 and myrTom. Robust myrTom expression confirms efficient Cre-mediated recombination following tamoxifen (tmx) administration at E14.5 and E15.5. Dotted lines indicate region of high magnification views in A.i and B.i. CPA1 expression was normal in mutant acinar cells. **C-D.i')** Representative vibratome sections of E17.5 control (C) and *Nf2*^{iAcinarKO} (D) pancreata stained for MUC1 and DBA, demonstrating normal lumenal morphology following post-morphogenetic deletion of MERLIN. **E-F.i")** Representative section IF of P25 control (E) and *Nf2*^{iInsKO} (F) pancreata following tmx induction at P2 and P3. *Nf2*^{iInsKO} animals display robust insulin expression and normal islet architecture following postnatal deletion of MERLIN in differentiated β-cells. These data show that MERLIN is required during a narrow developmental window but not for maintenance of differentiated fates. Representative images from n ≥2 animals per genotype. Scale bars: Panels A, B 50μm, A.i-B.i" 10μm, C, D 100μm, C.i-D.i" 10μm, E-F.i" 100μm.

Fig. S18. Loss of MERLIN alters Hippo- and PI3K-associated transcriptional programs in E14.5 pancreatic epithelium.

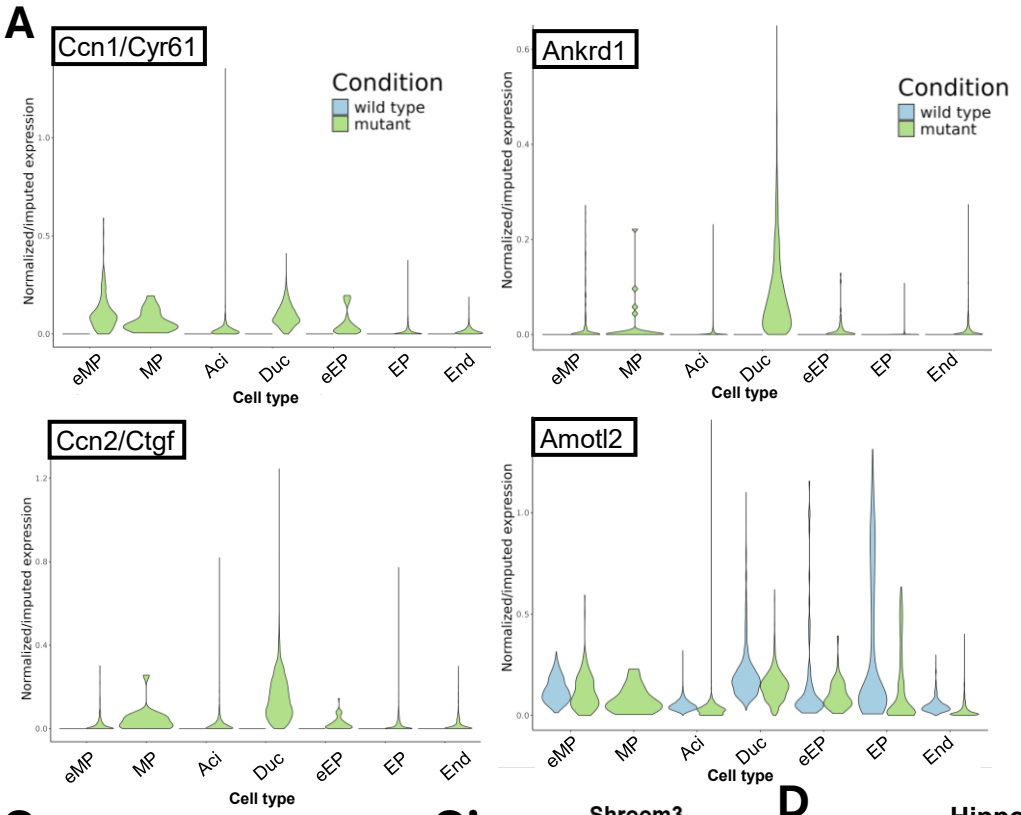

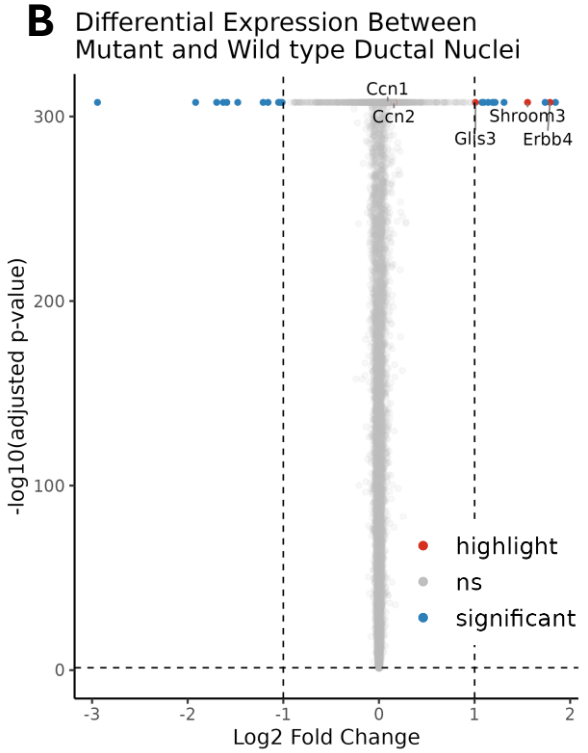

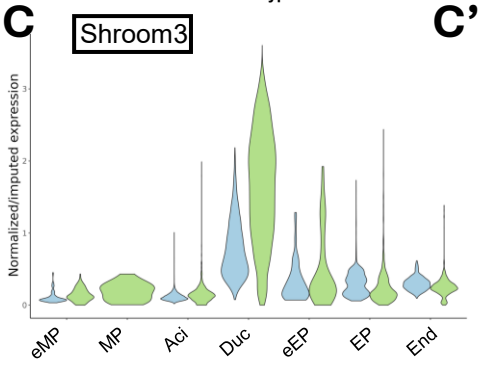

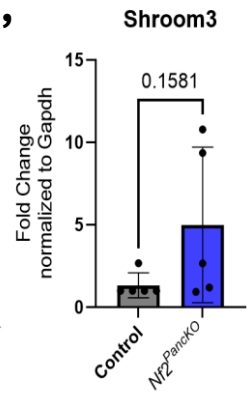

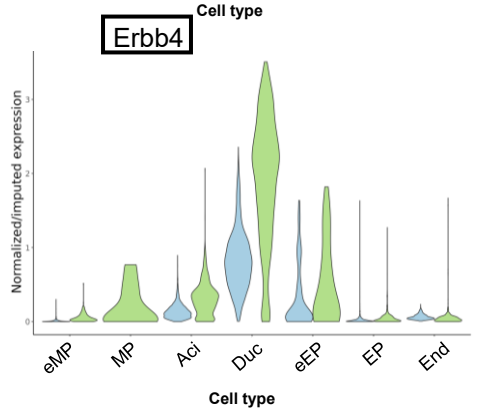

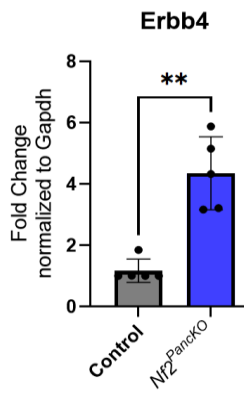

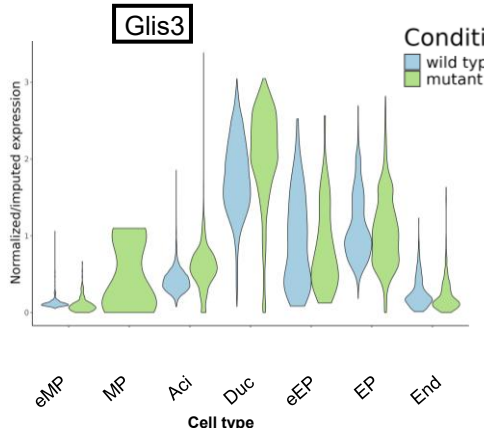

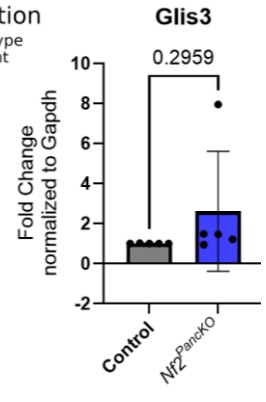

D

Hippo pathway upregulation in *Nf2*^{PancKO}

Ccn1	0.09147101	0.0624268	88.39805827	1.61	Canonical YAP target
Ccn2	0.15614977	0.08871859	80.91265752	1.51	Canonical YAP target
Ankrd1	0.09263006	0.05262901	55.69265339	1.36	Canonical mechanosensory YAP target
Pard3b	0.78863773	1.29404425	86.80910345	1.18	par polarity complex
Axl	0.01294206	0.01730129	29.45988207	1.2	YAP/TAZ-associated receptor target
Tead2	0.07948096	0.21476056	44.18115052	1.09	YAP/TAZ transcription factor primer
Magi1	1.09545638	2.67732637	115.1886937	2.14	polarity
Shroom3	1.55437365	1.09529199	113.0899743	1.22	actomyosin contracttility
Amotl2	0.07004856	0.12293387	39.16918609	1.14	YAP/TAZ sequestration factor
Wwc1	0.60883082	0.88058231	108.3665874	0.267	Hippo pathway mechanoregulator
Map4k3	0.4718327	0.83338925	81.18789913	0.233	Hippo pathway regulator

E

PI3K pathway upregulation in *Nf2*^{PancKO}

Gene	Log2FC	AveExpr	t (confidence)	FC	function
Igf1r	0.8316681	1.4779346	103.6990382	1.2	PI3K/AKT growth factor receptor
Igf2r	0.6738582	0.9847321	169.3530852	1.13	Growth factor trafficking
Fgfr2	1.0771672	1.7128578	154.4217008	1.14	Growth factor receptor signaling
Erbb4	1.7892603	1.3043235	124.3684537	1.17	EGF-family receptor signaling
Pdgfd	0.8450529	0.6366714	90.00646711	1.25	growth factor signaling
Pik3ap1	0.2052252	0.246531	87.58180801	1.16	PI3K adaptor
Pten	0.2222057	0.4356728	82.08692841	1.17	PI3K pathway regulator

F

FoxO4 pathway downregulation in *Nf2*^{PancKO}

Gene	Log2FC	AveExpr	t (confidence)	FC	function
Rps3a1	-1.0499975	1.32305308	-202.014052	0.483	ribosomal/ protein translation
Rps13	-0.635295	0.95710974	-139.8399274	0.644	ribosome biogenesis
Ppia	-0.6260485	1.32401234	-137.5467216	0.648	protein folding, stress, apoptosis
Naca	-0.6114122	0.82138562	-133.9125867	0.655	protein translation
Ptma	-0.6050032	1.62873044	-104.6738594	0.657	chromatin regulation
Rack1	-0.4813169	0.74917625	-149.0085641	0.716	scaffold for PKC, integrin, PI3K

G

Apoptosis downregulation in *Nf2*^{PancKO}

Gene	Log2FC	AveExpr	t (confidence)	FC	function
Nupr1	-0.4361442	0.22374374	-149.536537	0.739	stress induced apoptosis
Xbp1	-0.1193186	0.1176631	-83.45775133	0.921	
Ern1	-0.1526103	0.15983573	-72.61943207	0.9	secretory homeostasis
Rps27l	-0.318642	0.37198055	-105.115651	0.802	p53 associated stress /apoptosis
Cycs	-0.1020995	0.10869031	-61.39194422	0.932	cytochrome c, intrinsic apoptosis
Bax	-0.0643317	0.1437137	-39.61191386	0.956	mitochondial apoptosis
Trp53	-0.0480705	0.12508845	-33.01730018	0.967	stress surveillance /apoptosis

Fig. S18. Loss of MERLIN alters Hippo- and PI3K-associated transcriptional programs in E14.5 pancreatic epithelium. A) Violin plots showing upregulation of canonical Hippo pathway target genes, *cyr61, ankrd1, ctgf, and amotl2* in E14.5 in *Nf2*^{PancKO} pancreata. Violin plots made from integrated dataset (with only E14.5 control and mutant nuclei compared). **B-C)** Ductal nuclei from integrated dataset show significant upregulation of *glis3*, *shroom3*, and *erbb4*. **C')** qPCR validation of *shroom3*, *erbb4*, and *gli3s* in E14.5 control and mutant pancreata. Each dot represents one pancreas analyzed. Statistics by Welch's t-test, for Erbb4 p=0.002. Error bars indicate standard deviation. **D-G)** Gene set enrichment analysis (GSEA) of ductal nuclei shows activation of Hippo and PI3K-associated programs and repression of FoxO4 and apoptosis-associated programs in in *Nf2*^{PancKO} pancreata, as per the E14.5-only dataset (clustering as in Fig. S11A).

Fig. S19. Reduced YAP/TAZ dosage partially rescues pancreatic morphogenesis in *Nf2*^{PancKO} mice.

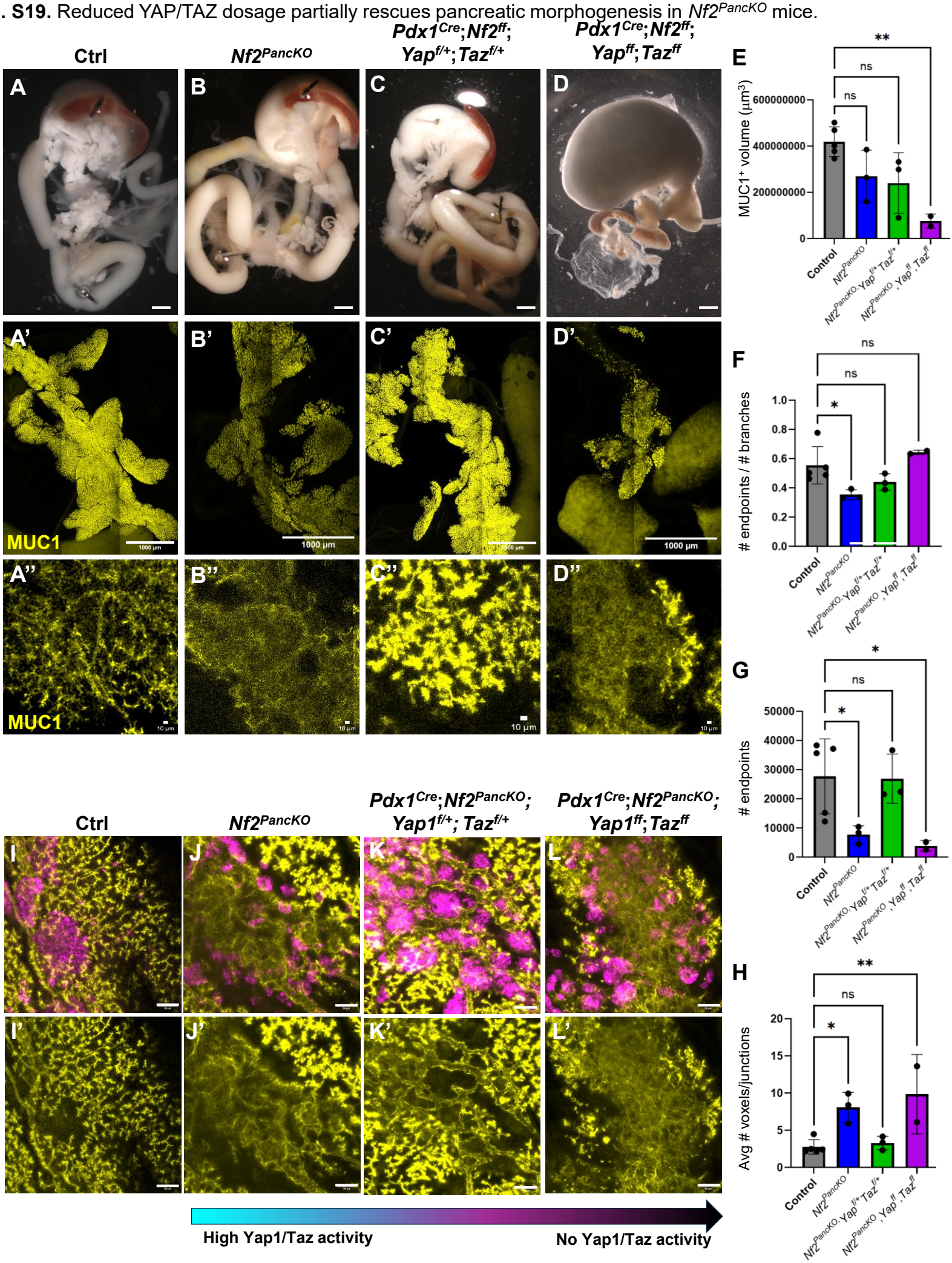

Fig. S19. Reduced YAP/TAZ dosage partially rescues pancreatic morphogenesis in *Nf2^{PancKO}* mice. A-D) Gross morphology of digestive tracts from control (A), *Nf2^{PancKO}* (B), *Nf2^{PancKO}Yap/Taz ^{Haploinsufficiency}* (C), and *Nf2^{PancKO}Yap/Taz^{PancKO}* (D) mice at P1. **A'-D'')** WMIF of MUC1 showing the pancreatic ductal network at P1 for each genotype, as indicated (A'-D', lower magnification. A''-D'', higher magnification). **E-H)** Quantification of various aspects of ductal lumen morphology. Each dot represents one pancreas evaluated. Data was analyzed by one-way ANOVA, followed by Dunnet's test for multiple comparisons. **E)** Total MUC1^{+} volume per pancreas. (P values: control vs *Nf2^{PancKO}* – 0.13, control vs *Nf2^{PancKO}Yap/Taz ^{Haploinsufficiency}* _ 0.07, control vs *Nf2^{PancKO}Yap/Taz^{PancKO}* _ 0.005). **F)** Number of terminal endpoints/total branches normalized to total branch number. (P values: control vs *Nf2^{PancKO}* – 0.03, control vs *Nf2^{PancKO}Yap/Taz ^{Haploinsufficiency}* _ 0.28, control vs *Nf2^{PancKO}Yap/Taz^{PancKO}* _ 0.55). **G)** Total number of terminal endpoints/pancreas. (P values: control vs *Nf2^{PancKO}* – 0.049, control vs *Nf2^{PancKO}Yap/Taz ^{Haploinsufficiency}* _ 0.99, control vs *Nf2^{PancKO}Yap/Taz^{PancKO}* _ 0.04). **H)** Mean junction size. (P values: control vs *Nf2^{PancKO}* – 0.02, control vs *Nf2^{PancKO}Yap/Taz ^{Haploinsufficiency}* _ 0.97, control vs *Nf2^{PancKO}Yap/Taz^{PancKO}* _ 0.0096). Reduction of YAP/TAZ dosage partially restores ductal architecture in mutant pancreata. **I-L)'** Higher magnification images of the central epithelium from each genotype stained for MUC1 together with insulin (INS) and glucagon (GLU). Scale bars: Panels A-D 500μm, A'-D' 1000μm, A''-D'' 10μm, I-L' 50μm. For all graphs, error bars indicate standard deviation.

Fig. S20. Loss of MERLIN alters transcriptional programs regulating polarized membrane trafficking.

A

Vesicular trafficking / polarity genes increased in *Nf2*^{PancKO}

Gene	Log2FC	AveExpr	t (confidence)	Fold cha	function
Magi1	1.09545638	2.67732637	115.1886937	2.14	polarity
Pard3	0.24472682	1.34334155	28.11418682	1.73	par polarity complex
Pard3b	0.78863773	1.29404425	86.80910345	1.18	par polarity complex
Exoc1	0.12665634	0.11731518	74.45384255	1.09	exocyst trafficking
Exoc4	0.0916534	0.8844696	13.63448572	1.06	exocyst trafficking
Vps13b	0.1361309	0.5629195	29.18005713	1.1	vesicle trafficking
Vps13a	0.07040746	0.20079005	36.82635436	1.05	vesicle trafficking
Vps33a	0.08330448	0.06789836	63.89366939	1.05	vesicle trafficking
Rab8b	0.08178121	0.1035554	63.90395116	1.05	Rab trafficking
Rab1a	0.07780086	0.19795923	40.88762463	1.06	Rab trafficking
Rab5a	0.0608453	0.12572187	43.97736659	1.06	Rab trafficking
Ap2b1	0.12183358	0.22907743	65.95966381	1.09	Clathrin adaptor
Ap2a2	0.06154232	0.13434775	47.06574384	1.04	Clathrin adaptor
Ap3b1	0.07673425	0.27858103	36.8965155	1.05	Clathrin adaptor
Snx24	0.09094548	0.50483343	25.92312475	1.06	sorting nexin
Snx27	0.06684482	0.15280013	40.48132717	1.05	sorting nexin
Snx2	0.06191888	0.14966343	45.2389188	1.04	sorting nexin
Stx3	0.07674173	0.10199616	48.94494016	1.06	SNARE trafficking
Cdc42se	0.06626551	0.20853842	31.41802484	1.05	Cdc42 polarity pathway
Pik3ap1	0.20522519	0.24653105	87.58180801	1.16	PI3K pathway
Pten	0.22220572	0.43567277	82.08692841	1.17	PI3K pathway

B

Secretory / membrane trafficking genes downregulated in *Nf2*^{PancKO}

Gene	Log2FC	AveExpr	t (confidence)	Fold change (FC)	function
Rab2a	-0.1603329	0.43316835	-63.57449951	0.89	Rab trafficking
Arf1	-0.0802102	0.30792567	-35.868511	0.95	Arf trafficking
Arf4	-0.1249238	0.4097214	-50.06708546	0.92	Arf trafficking
Clta	-0.1192491	0.23090834	-65.95558147	0.92	Clathrin trafficking
Lamp1	-0.1349383	0.31264318	-55.77684874	0.91	Lysosome/endosome
Sort1	-0.0605265	0.19960083	-26.78613487	0.96	Sorting
Sec11a	-0.1415552	0.43280712	-56.42768414	0.91	translocation
Sec61b	-0.2554412	0.32819044	-102.2528114	0.83	translocation
Sec62	-0.0959503	0.49550404	-35.80820619	0.93	ER trafficking

C

Junctional genes dysregulated in *Nf2*^{PancKO}

Gene	Log2FC	AveExpr	t (confidence)	Fold change (FC)	function
Cldn3	-0.5043347	0.5243957	-149.47963	0.71	Tight junction
Cldn7	-0.2557378	0.36606451	-103.6090372	0.83	Tight junction
Cldn10	-0.2819441	0.36295505	-108.6849955	0.82	Tight junction
Cldn6	-0.1327914	0.17046681	-77.70276026	0.92	Tight junction
Ocln	-0.1570066	0.1875064	-78.46254698	0.9	Tight junction
Tjp1	0.23204897	0.34365259	80.83331687	1.18	tight junction (ZO-1)
Tjp2	0.11778806	0.34078149	43.13380629	1.09	tight junction

D

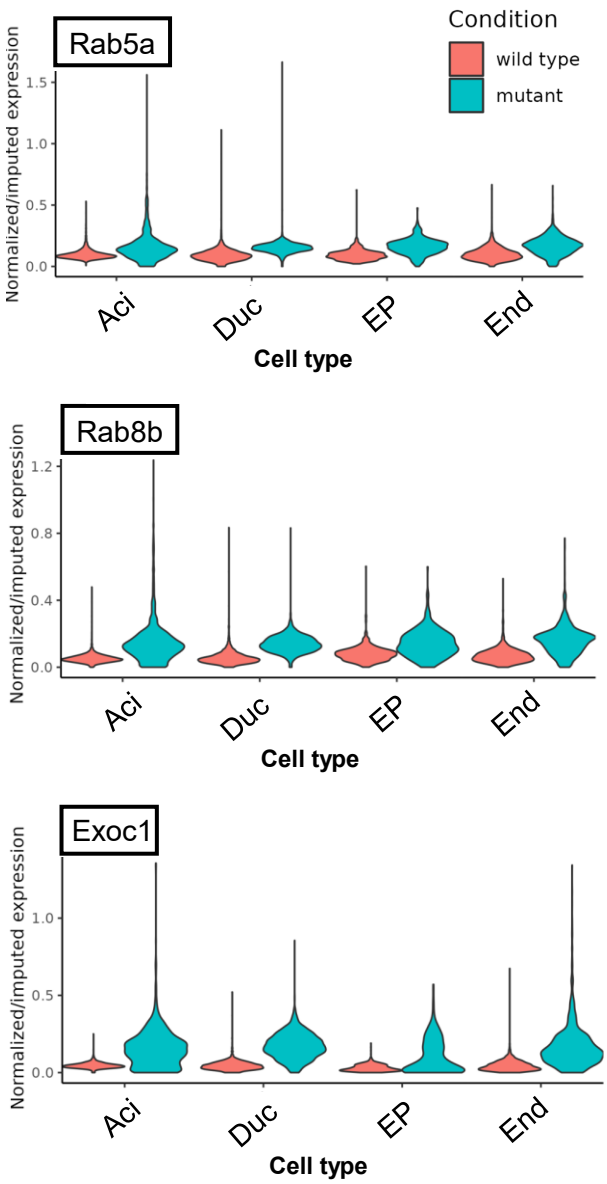

Fig. S20. Loss of MERLIN alters transcriptional programs regulating polarized membrane trafficking. A-C) Key trafficking, secretory, and junctional genes are dysregulated in *Nf2*^{PancKO}, in E14.5 ductal nuclei (clustering as in Fig. S10). **D)** Violin plots showing expression of selected vesicle trafficking genes in E14.5 control and mutant ductal nuclei (E14.5-only data set, clustering as in Fig S11A).

Fig. S21. Genetic hyperactivation of PI3K signaling phenocopies defects observed in *Nf2*^{PancKO} pancreata.

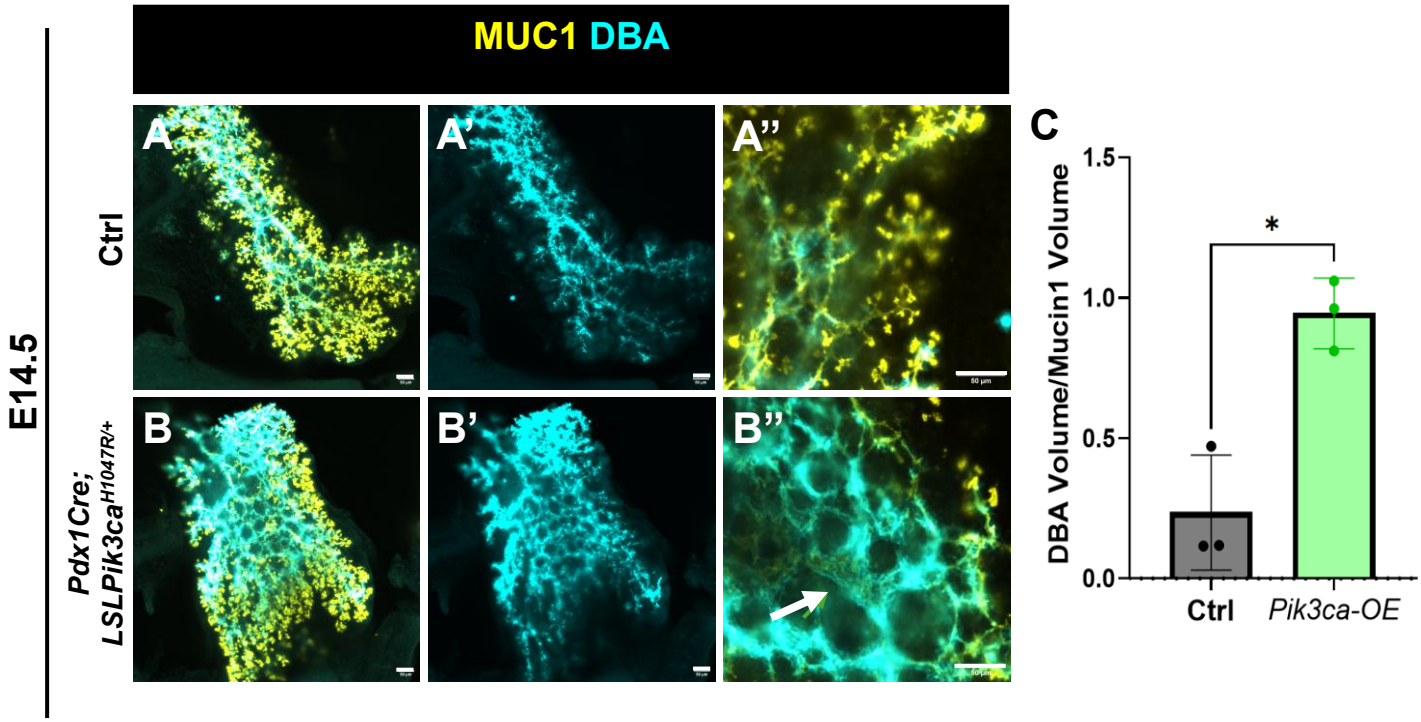

Fig. S21. Genetic hyperactivation of PI3K signaling phenocopies the epithelial remodeling defects of *Nf2*^{PancKO} pancreata. **A-B)** WMIF for DBA and MUC1 showing MIPs of 100μm substacks through the central region of control **(C)** and *Pdx1*^{Cre}*;LSL-Pik3ca*$^{H1047R/+}$ **(D)** pancreata. **A', B")** Optical section at high magnification. Constitutive PI3K activation results in enlarged, dysmorphic ducts (white arrows), closely phenocopying the epithelial defects observed in mutants. Representative images from n=3 embryos/genotype. Scale bars: Panels A-B"' C-D" 50μm. **C)** Quantification of DBA volume/MUC1 volume, each dot represents a single pancreas evaluated. P=0.0112 by Welch's t-test.

Fig. S22. Hyperactivation of PI3K results in apical membrane disorganization, which excess intracellular Crb3.

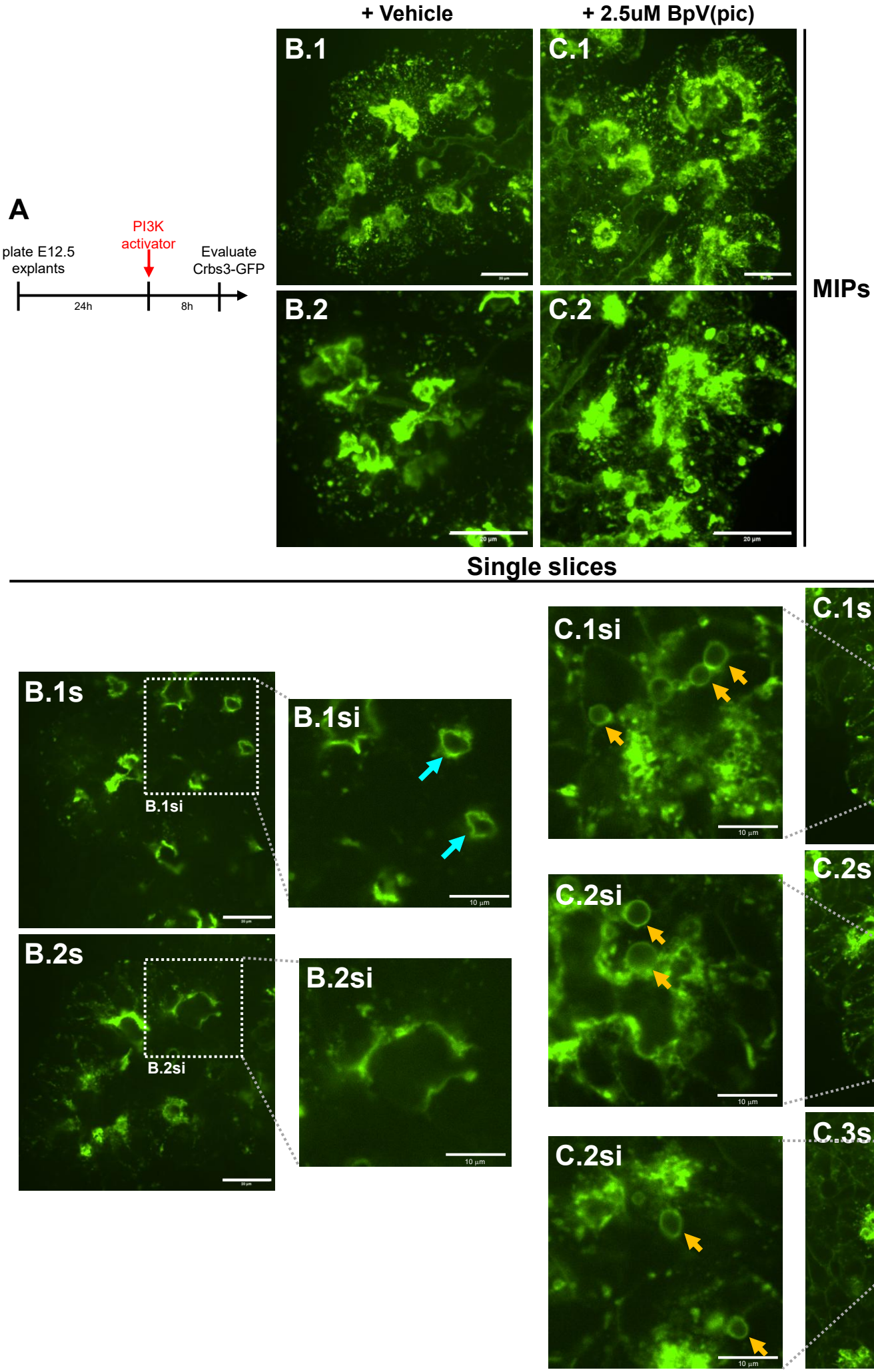

Fig. S22. Hyperactivation of PI3K results in apical membrane disorganization, which excess intracellular Crb3. **A)** Experimental schematic; Control (*Pdx1Cre, Crb3^{GFP})* pancreata were explanted at E12.5 and cultured for 24 hours prior to drug addition. Pancreata were treated with either vehicle or 2.5uM BpV(pic) for 8 hours and then live imaged. MIPS of control **(B.1-B.2)** and BpV(pic) treated **(C.1-C.2)** explants. Single optical sections from control **(B.1s-B.2s)** and BpV(pic) treated **(C.1-C.3s)** pancreata. Cyan arrows, lumens; Orange arrows, aberrant apical membrane or vesicles. Dashed box indicates region of interest highlighted in B.1si – C3.si. Note disorganization of Crb3 near the apical membrane.

Fig. S23. Distinct cortical signaling domains in wild type E11.5 pancreatic epithelium marked by MERLIN, EZRIN or PI3K.

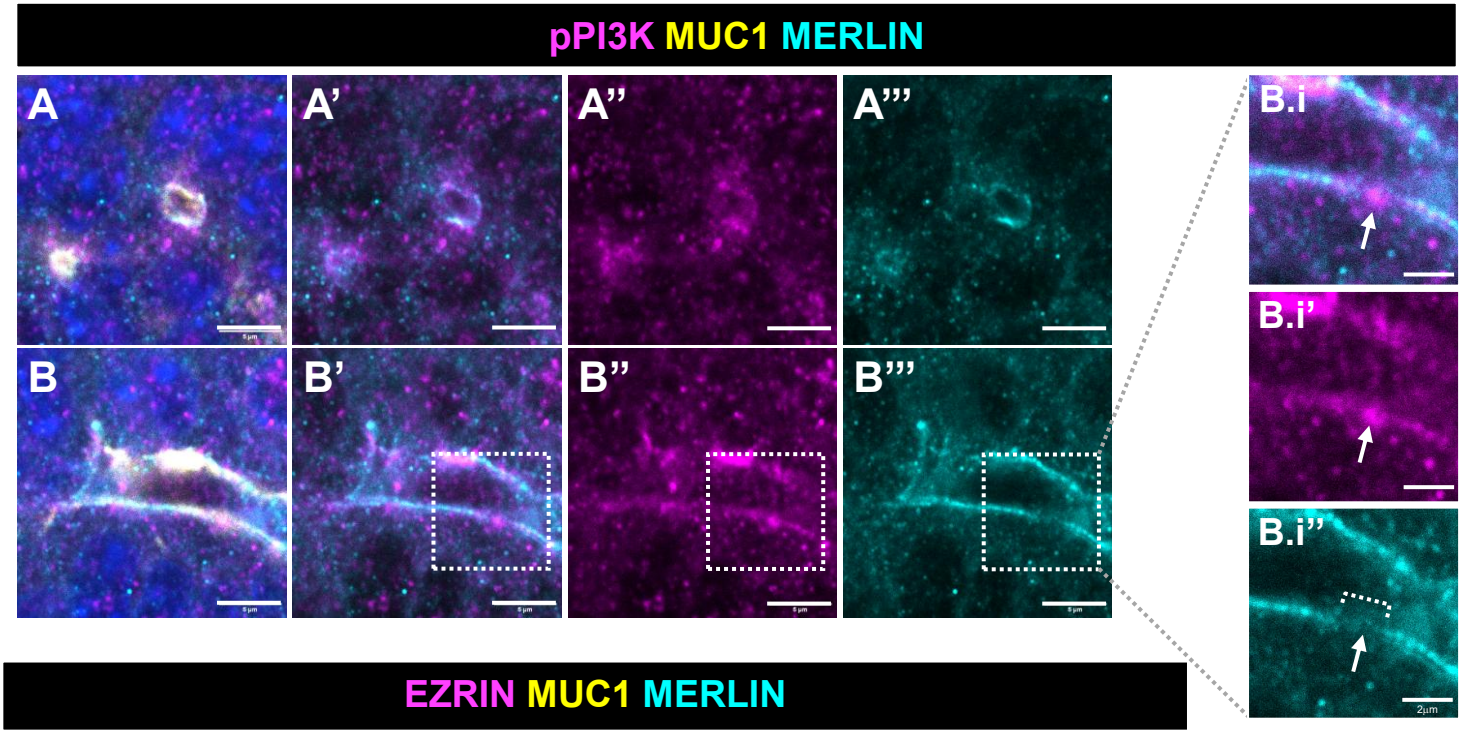

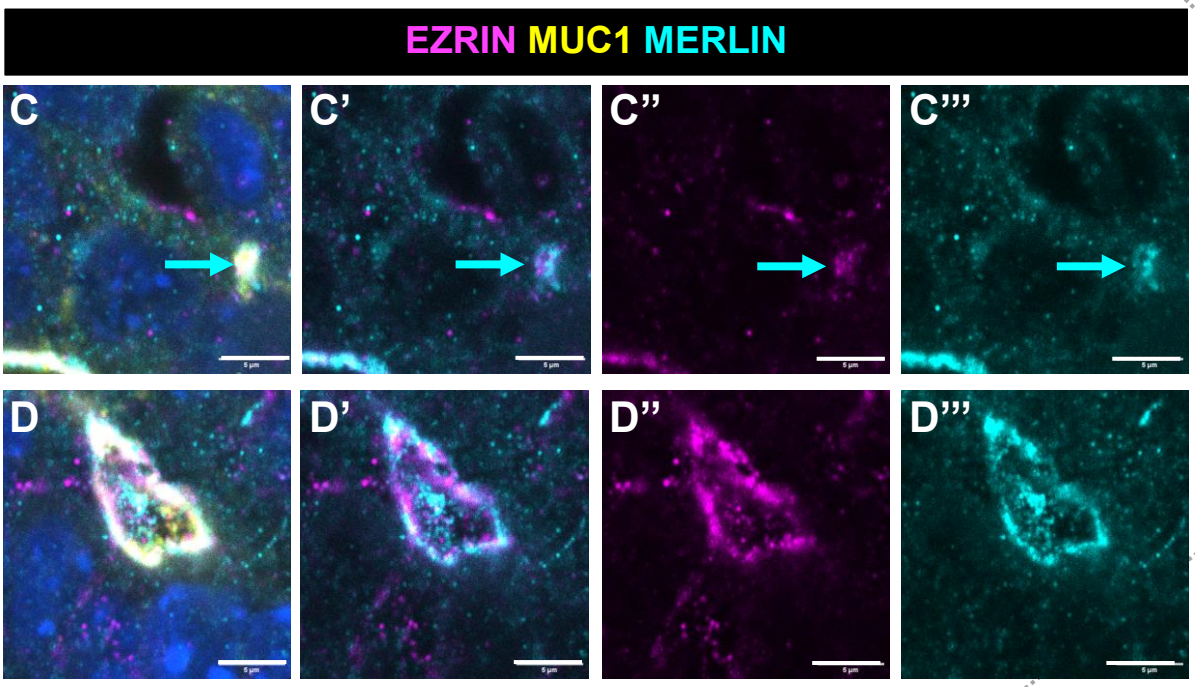

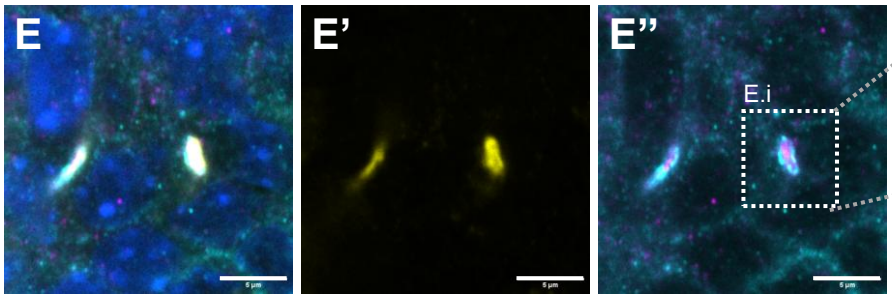

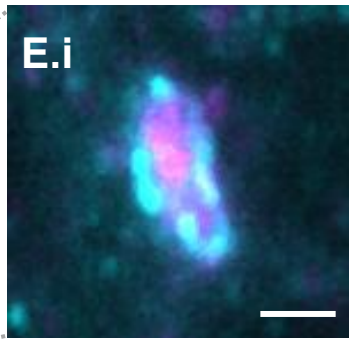

G

AMIS	total	Merlin Only +	Ezrin Only +	Dual Positive
# Muc1 negative	14	0	6	8
# Muc1 positive	51	1	4	46

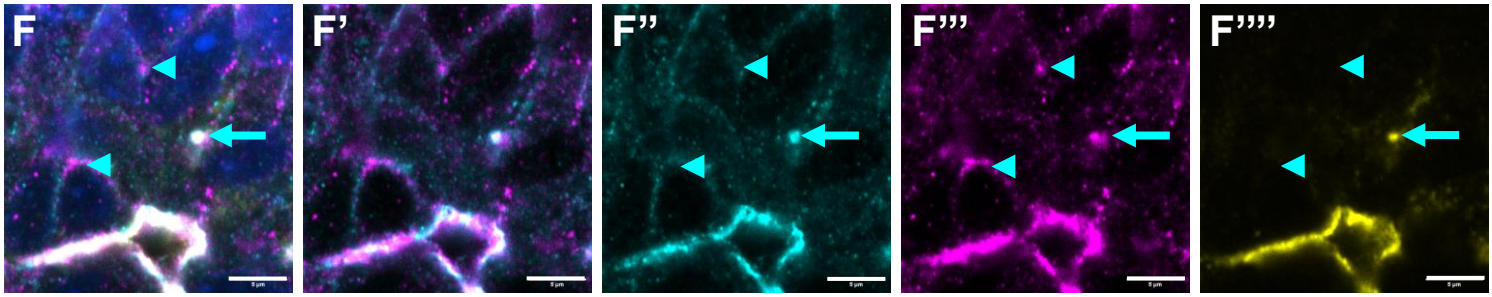

Fig. S23. Distinct cortical signaling domains in wild type E11.5 pancreatic epithelium marked by MERLIN, EZRIN or PI3K. A-B’’’) IF for phosphorylated PI3K (antibody against phospho-p85/p55), MERLIN, and MUC1 in wildtype E11.5 pancreata. Both pPI3K and MERLIN are apically localized at **(A-A’’’)** nascent and **(B-B’’’)** open/mature lumens. **B.i-B.i’’)** High magnification insets of open lumen in B-B’’’. White arrow indicates region of high pPI3K immunoreactivity, and relatively low MERLIN signal. **C-C’’’)** IF for EZR, MERLIN and MUC1 in wildtype E11.5 pancreata at a nascent lumen, and **D-D’’’)** and open lumen. **E)** At select nascent lumens in E11.5 wildtype tissue, MERLIN appeared to be localized in a ring around EZR (**E.i)**. **F)** MERLIN and EZRIN localization at an early AMIS (MUC1-negative, cyan arrowhead) and more developed AMIS (MUC1-positive, cyan arrow). **G)** Extended data for Fig 4.X, showing number early and developed AMIS evaluated for MERLIN and EZR localization across three pancreata. Scale bars: All panels 5μm, except E.i which is 1μm.

.

Fig. S24. MERLIN and mechanotransduction-associated pathways respond to epithelial cell density.

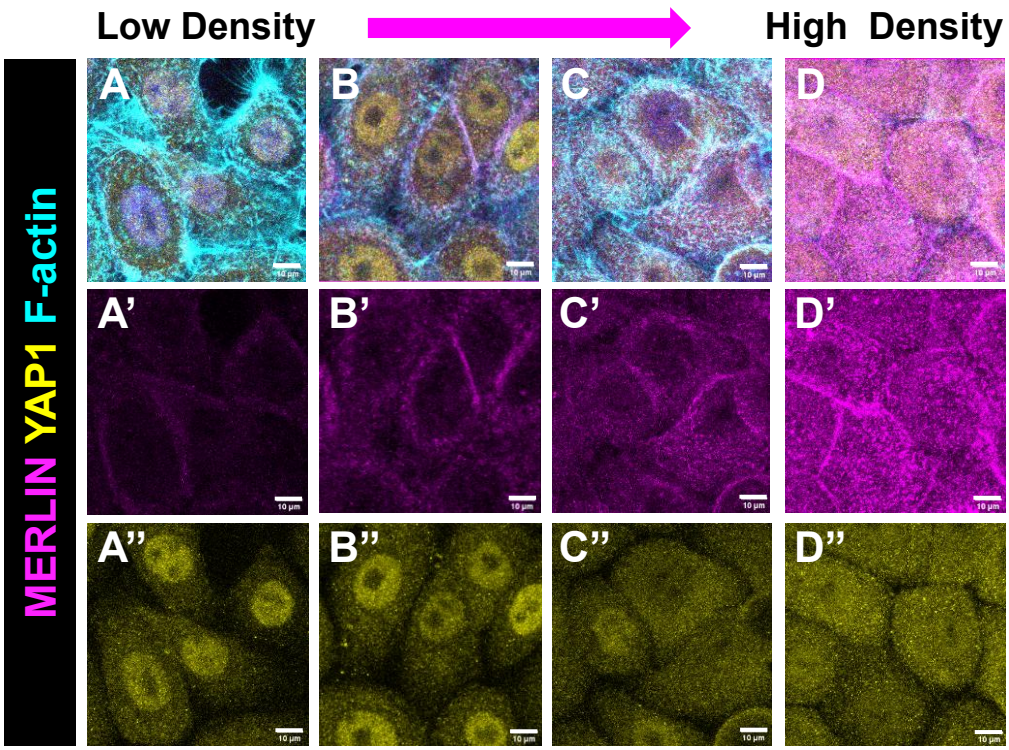

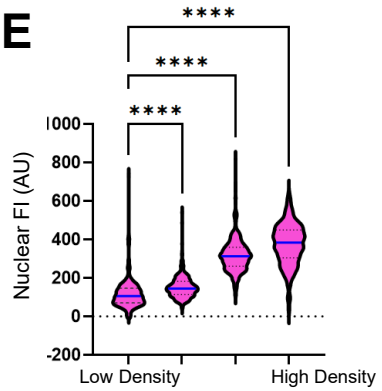

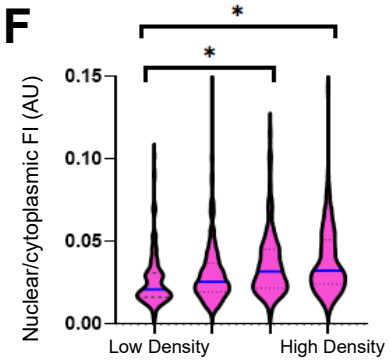

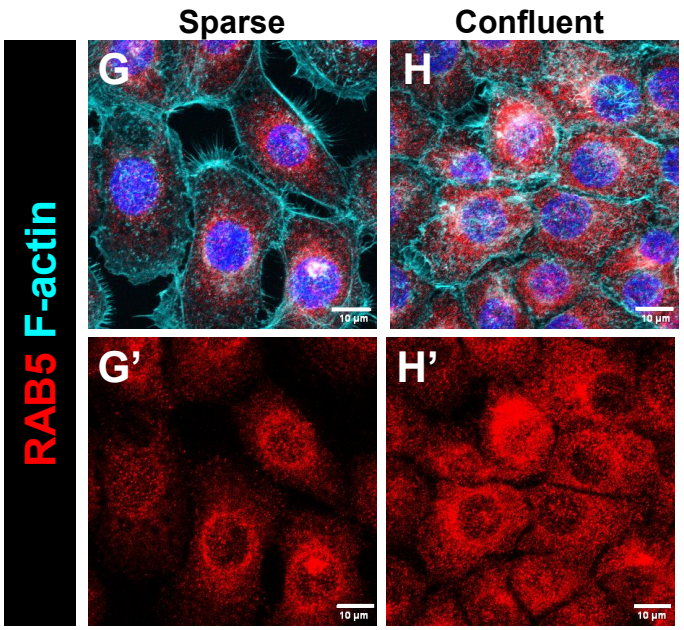

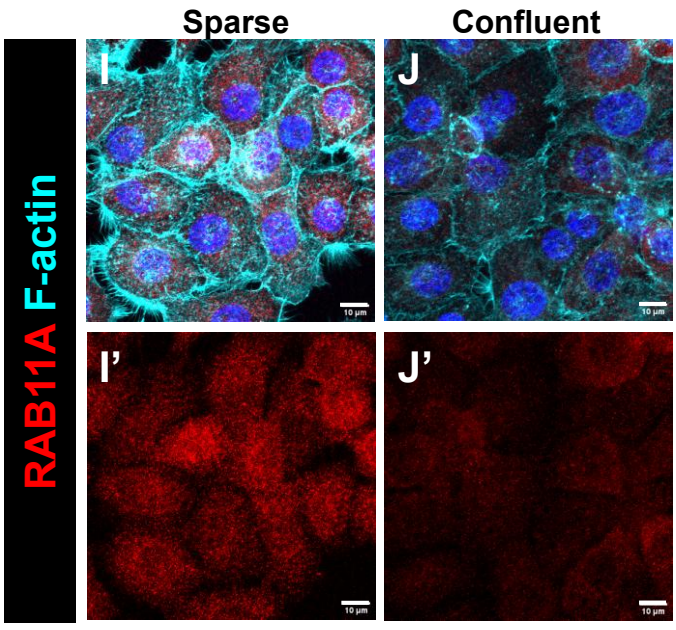

K

Mechanotransduction pathways

Gene	Log2FC	AveExpr	t (confidence)	Fold change (FC)	function
Pkhd1l1	0.00500757	0.00738898	9.723786368	1.38	tubular mechanosensation
Sorbs2	1.30823201	1.40678897	122.2675175	0.542	mechanical adaptor actin linkage
Shroom3	1.55437365	1.09529199	113.0899743	1.22	actomiyosin contracttility
Lpp	0.57848412	1.18745173	76.68822348	0.184	force-responsive adhesion signaling
Pkp4	0.53197013	0.76122327	90.80998854	0.388	junctional tension organization
Prkg1	0.81588652	0.59867452	77.29170883	0.147	cytoskeletal signaling kinase
Spata13	0.56419451	0.68181033	102.509109	0.321	Rho family GTPase signaling
Map4k3	0.4718327	0.83338925	81.18789913	0.233	Hippo pathway regulator
Wwc1	0.60883082	0.88058231	108.3665874	0.267	Hippo pathway mechanoregulator

Fig. S24. MERLIN and mechanotransduction-associated pathways respond to epithelial cell density. A-D) Human pancreatic ductal epithelial (HPDE) cells cultured at 10,000 cells/cm^2 (A), 20,000 cells/cm^2 (B), 30,000 cells/cm^2 (C), or 50,000cells/cm^2 (D) and stained for MERLIN, YAP1, and F-actin. Increasing cell density (increased intracellular tension) results in elevated nuclear MERLIN localization. **E)** Quantification of nuclear MERLIN fluorescence intensity (FI). (Data analyzed by Anova followed by Dunnett's test for multiple comparisons. P <0.001 for all comparisons). **F)** Quantification of nuclear/cytoplasmic MERLIN fluorescence ratio. (Data analyzed by Anova followed by Dunnett's test for multiple comparisons. P = 0.10 for seeding density of 10,000cells/cm^2 vs 20,000cells/cm^2, p = 0.0002 for 10,000cells/cm^2 vs 30,000cells/cm^2, p <0.0001 for 10,000cells/cm^2 vs 50,000cells/cm^2. For E-F, n >100 cells analyzed per condition). For E-F, blue line indicated median of data. **G, H)** IF for RAB5 in sparse (G) or confluent (H) HDPE cultures. **I)** Quantification of MERLIN expression FI in G, H. **J-K')** IF for RAB5 in sparse (J) or confluent (K) HDPE cultures. **L-M')** IF for RAB11 in sparse (G) or confluent (H) HDPE cultures. Cell density alters intracellular localization of both RAB5 and RAB11, consistent with density-dependent regulation of membrane trafficking. **N)** Selected mechanotransduction-associated genes are differentially expressed in E14.5 *Nf2*^{PancKO} ductal nuclei relative to controls (clustering as in Fig S11). All scale bars 10μm.